AD-A108 208 FOREIGN TECHNOLOGY DIV WRIGHT-PATTERSON AFB OH F/G 20/4
ACTA MECHANICA SINICA (SELECTED ARTICLES).(U)
NOV 81
UNCLASSIFIED FTD-ID(RS)T-0708-81 NL

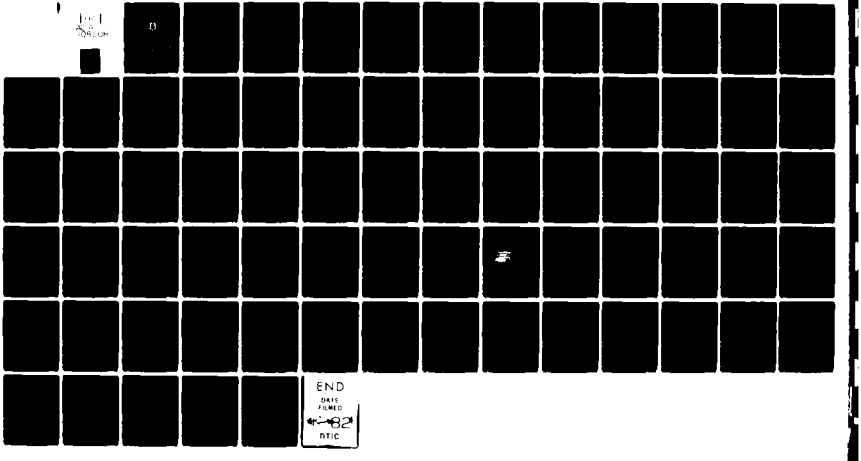

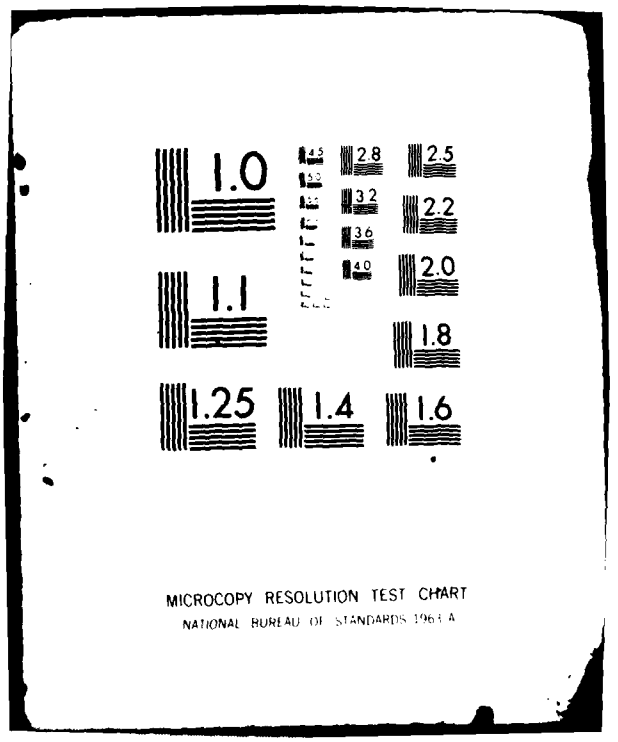
1.0
1.1
1.25
1.4
1.6
1.8
2.0
2.2
2.5
2.8
3.2
3.6
4.0
MICROCOPY RESOLUTION TEST CHART
NATIONAL BUREAU OF STANDARDS 1963 A

FTD-ID(RS)T-0708-81

FOREIGN TECHNOLOGY DIVISION

ACTA MECHANICA SINICA
(Selected Articles)

Approved for public release;
distribution unlimited.

EDITED TRANSLATION

FTD-ID(RS)T-0708-81 12 November 1981

MICROFICHE NR: FTD-81-C-001025

ACTA MECHANICA SINICA (Selected Articles)

English pages: 70

Source: Acta Mechanica Sinica, Nr. 1, 1980, pp. 18-28, -8-47, 84-99

Country of origin: China
Translated by: SCITRAN
F33657-78-D-0619
Requester: FTD/TQTD

PREPARED BY:

TRANSLATION DIVISION
FOREIGN TECHNOLOGY DIVISION
WP-AFB, OHIO.

TABLE OF CONTENTS

Numerical Calculation of Steady Two-dimensional Axi-symmetrical Turbulent Boundary Layer of a Compressible Fluid

Wang Ying-shih

(Institute of Mechanics, Academia Sinica)

This paper employed a momentum equation expressed by the stress tensor to derive the momentum equation of a non-rotational steady axi-symmetrical turbulent boundary layer of a compressible fluid in the axi-symmetrical coordinate system. It was found that if the flow in the duct was to be treated as viscous fluid everywhere then the curvature of the duct and the rate of variation of the curvature along the direction of the flow cannot be too large. This has not been proven in any existing literature.

Based on the set of equations proposed in this paper, we compiled a program and computed an example.

SYMBOLS

A	cross-sectional area
A, B, C	coefficients of Φ difference equations
A_u, B_u, C_u	coefficients of the velocity u difference equations
A', B'	coefficients of transformation
a, b	coefficients of the conduction terms in the conventional conservation equations
c	coefficient of the diffusion term in conventional conservation equations.
d	source term in the conventional conservation equations
F'	friction face per unit length of the wall on the fluid

g_1, g_2, g_3, g_4, g_5, g_6	coefficients of relevant terms in the derivation of the difference equations
H_i	heat of formation of the i^{th} component
h	enthalpy
h_1, h_2, h_3	Lame coefficient
J	flux in the positive y direction
l	mixing length
$\dot{m}''$	mass transfer rate
m_i	mass fraction of chemical reaction composition
N	number of nodal points crossing the stream line
p	pressure intensity
R	gas constant
S_1, S_2, S_3, S_4	relevant coefficients of the source terms in the difference equation of velocity u.
T	absolute temperature
u	velocity component corresponding to the x-direction
V	velocity vector
v	velocity component corresponding to the y direction, velocity component corresponding to the r direction
v_1, v_2, v_3	velocity components with respect to the α, β, γ increasing direction
x, y, θ	axi-symmetrical coordinate system
y_1	characteristic thickness of the boundary layer
α, β, γ	conventional orthogonal coordinate system
k	curvature at boundary I
π_{ij}	stress tensor
τ_{ij}	viscous stress tensor
δ_{ij}	Kronecker δ
μ	dynamic viscosity coefficent
p	density
σ_h	Prandtl number
σ_i	Schmidt number

τ	shear stress
Φ	conventional strain quantity
ψ	flow function
ω	non-dimensional flow function
ϑ	refer to Figure 1 for definition
上标:	superscript
*	retardation value
下标:	subscript
d	in the duct
$\left.\begin{matrix} D, D^+, D^-, DD^+, DD^- \\ u, u^+, u^-, uu^+, uu^- \end{matrix}\right\}$	nodal points controlling the difference on the volumetric boundary
E	outer boundary
f	occupied by the fluid
h	thermal
l	inner boundary
j	chemical composition i
t	turbulent
eff	effective

This paper was received on June 14, 1978.

In the actual fluid flow process, especially under heat transfer and mass transfer conditions, the effect of viscosity is very important. Furthermore, most of the viscous flow process is a turbulent flow. Therefore, in order to solve this type of a flow process perfectly it must begin with the solution of the turbulent viscous flow equation set. However, the work load involved in obtaining solution to this set of equations is rather large. Until the late sixties with the development of computational methods and computers it was then possible to work in this area.

The viscous flow problem can be divided into viscous flow with return flow and the boundary layer flow without return flow. These two types of flow have different types of basic equations. Their solution and the treatment of boundary conditions are not the same[1-3]. This paper mainly discussed the calculation of fluid field of the turbulent boundary layer of a compressible fluid in a two-dimensional axi-symmetrical coordinate system.

I. Basic Equations and Discussion of the Content

When a compressible fluid undergoes non-rotational axi-symmetrical flow in a axi-symmetrical coordinate system as shown in Figure 1, the boundary layer kinetic equations under steady state are shown as follows (detailed derivation see Appendix 1):

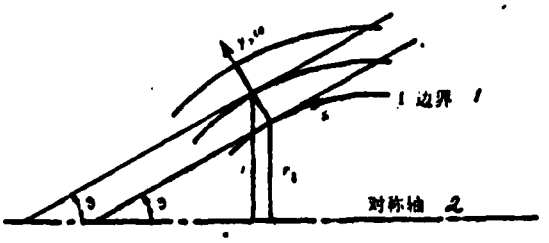

Figure 1. Axi-symmetrical coordinate system. Key: 1. boundary, 2. axis of symmetry.

continuity equation $$\frac{\partial}{\partial x}(\rho r u) + \frac{\partial}{\partial y}(\rho r v) = 0 \tag{1}$$

momentum equation $$\rho u \frac{\partial u}{\partial x} + \rho v \frac{\partial u}{\partial y} = \frac{1}{r}\frac{\partial}{\partial y}(\tau r) - \frac{dp}{dx} \tag{2}$$

mass transfer equation $$\rho u \frac{\partial m_i}{\partial x} + \rho v \frac{\partial m_i}{\partial y} = -\frac{1}{r}\frac{\partial}{\partial y}(J_i r) + R_i \tag{3}$$

energy equation $$\rho u \frac{\partial h^*}{\partial x} + \rho v \frac{\partial h^*}{\partial y} = -\frac{1}{r}\frac{\partial}{\partial y}\left\{\left(J_h + \sum_1^n H_i J_i - u\tau\right) r\right\} \tag{4}$$

If the fluid satisfies the conditions of a gas completely, then

$$\frac{p}{\rho} = RT \tag{5}$$

If we neglect the variation of C_p for each component and also neglect v^2, then the stationary enthalpy can be defined as:

$$h^* = C_p T + \sum_1^n H_i m_i + \frac{u^2}{2} \tag{6}$$

The above equations are applicably in the laminar flow region of the boundary layer as well as in the turbulent region of the boundary layer. When it is used for turbulent boundary layer, all the physical quantities should be expressed using the time average values.

At the moment let us assume that the momentum, mass transfer, and heat transfer respectively obey Newton's law, Fisk's law, and Fourier's law in the turbulent boundary layer similar to what happens in the laminar flow boundary layer. The exchange coefficient in the entire boundary layer can be expressed using the effective values, i.e.

$$\tau = \mu_{eff}\left(\frac{\partial u}{\partial y}\right) \tag{7}$$

$$J_i = -\left(\frac{\mu_{eff}}{\sigma_{i\,eff}}\right)\left(\frac{\partial m_i}{\partial y}\right) \tag{8}$$

$$J_h = -\left(\frac{\mu_{eff} C_p}{\sigma_{h\,eff}}\right)\left(\frac{\partial T}{\partial y}\right) \tag{9}$$

In the layer flow region μ_{eff}, $\sigma_{h\,eff}$, and $\sigma_{i\,eff}$ correspond to the viscosity, Prandtl number, and Schmidt number of the fluid, respectively. The effect viscosity inside the turbulent flow region is defined by adopting the mixing length concept of Prandtl which is:

$$\mu_{eff(t)} = \rho l^2 \left|\frac{\partial u}{\partial y}\right| \tag{10}$$

and $\sigma_{h\,eff}$ and $\sigma_{i\,eff}$ are the effective turbulent flow Prandtl number and the effect turbulent flow Schmidt number, respectively.

Equations (2), (3), and (4) are of the conservation equation type. The left hand side of the equal sign is the convection term. The first term on the right is the diffusion term and the second term is the source. If the source term is known or can be obtained through another expression, then the above ten equations can give solution to the ten unknowns $\rho, T, h^*, u, v, m_i, \tau, J_i, J_h, \mu_{eff}$. During the solution seeking process the values for $l, \sigma_{i\,eff}, \sigma_{h\,eff}$ can be obtained from certain expressions or experimental data[2].

In order to obtain the solution more conveniently, let us transform the above equations into the von Mises coordinate system (x-ψ coordinate system) and bring in the concept of the flow function.

$$\frac{\partial \psi}{\partial y} = \rho r u, \quad \frac{\partial \psi}{\partial x} = -\rho r v \tag{11}$$

Because

$$\left(\frac{\partial}{\partial x}\right)_y = \left(\frac{\partial}{\partial x}\right)_\psi - \rho r v \left(\frac{\partial}{\partial \psi}\right)_x \tag{12}$$

$$\left(\frac{\partial}{\partial y}\right)_x = \rho r u \left(\frac{\partial}{\partial \psi}\right)_x \tag{13}$$

Equations (2), (3), and (4) then become

$$\frac{\partial u}{\partial x} = \frac{\partial}{\partial \psi}(\tau r) - \frac{1}{\rho u}\frac{dp}{dx} \tag{2'}$$

$$\frac{\partial m_j}{\partial x} = -\frac{\partial}{\partial \psi}(J_j r) + \frac{R_j}{\rho u} \tag{3'}$$

$$\frac{\partial h^*}{\partial x} = -\frac{\partial}{\partial \psi}\left\{\left(J_h + \sum_i^{\cdot} H_i J_i - u\tau\right) r\right\} \tag{4'}$$

Because equations (7), (8), and (9) can be transformed into partial derivatives with respect to τ, J_j, and J_h respectively, therefore equations (2'), (3'), and (4') become the classical parabolic curve equation with a source. Henceforth, it is in principle possible to adopt numerical methods which are suitable for parabolic equations to process the above set of equations.

Before proceeding further in seeking for the solutions of the above equations, we are going to carry out a discussion on the above mentioned momentum equation.

In the derivation of momentum equation in the axisymmetrical coordinate system (see Appendix I), the first obtained equation is

$$\rho u \frac{\partial u}{\partial x} + \rho v \frac{\partial u}{\partial y} = \frac{\partial \tau}{\partial y} + \frac{\cos\vartheta}{r}\tau - \frac{\partial p}{dx} \tag{I-4}$$

Only general boundary layer assumptions are made in the deviation process. The applicable region of equation (I-4) is relatively wider. It can be applied not only to the boundary layer flow of a revolving surface on the basis of the axi-

symmetrical coordinates, but also to the jet boundary layer flow on the basis of cylindrical coordinates.

As for the analysis of axi-symmetrical jet flow it is generally better to use the cylindrical coordinate system. At this time the thickness of the boundary layer and the radial length belong to the same order of magnitude. Therefore, the momentum equation of the boundary layer of a steady two-dimensional axi-symmetrical jet flow can be derived

$$\rho u \frac{\partial u}{\partial x} + \rho v \frac{\partial u}{\partial r} = \frac{1}{r} \frac{\partial}{\partial r} (\tau r) - \frac{dp}{dx} \qquad (14)$$

where u and v are the velocity components along the x and r directions, respectively.

Comparing equation (I-4) with equation (14) and also referring to Figure 1, we can see that when $\vartheta \to 0$ and $r_1 \to 0$ the orthogonal axi-symmetrical curve coordinate system is reduced to a cylindrical coordinate system. Equation (I-4) becomes equation (14). Earlier Mangler, in his treatment of the laminar boundary layer problems, did not keep the second term on the right hand side of equation (I-4) through order of magnitude comparison. Mathematically, it transformed the boundary layer problem of a revolved body into a planar boundary layer problem for processing in order to simplify the procedure necessary to obtain the solution[5]. Presently, because of the use of numerical computations and through the establishment of computational programming based on the equations stated above, we not only can solve the boundary layer problem of a revolved body but also can deal with the boundary layer problem of the axi-symmetrical jet flow and the boundary layer problem of the planar flow.

In order to raise the accuracy of calculation in the various regions in the boundary layer, the choice of the difference net-

work before the establishment of the difference equations is very important. If we use the simple x-ψ coordinate system to establish the network then in the region where x is small it is not possible to clearly express the variation of the flow field due to the small number of network nodal points. If for this reason the coordinate lines for ψ value becomes much more dense in order to have more nodal points in the x direction in the area where x is small, then there are large number of unnecessary nodal points in the area where x is large.

In overcoming the above difficulty, some authors used the $x - u/u_E$ or $x - y/y_E$ coordinate system. In this paper we used the Patankar-Spalding coordinate system mentioned in Reference [2] which is the x-ω coordinate system. This type of method which transforms the ordinate of the orthogonal coordinate system into a relative value is to arrange so that the number of network nodal point to be the same during every step as the computation progresses in order to improve the accuracy of the computation in the area where x is small. Based on Reference [2]

$$\omega = \frac{\psi - \psi_1}{\psi_E - \psi_1} \tag{15}$$

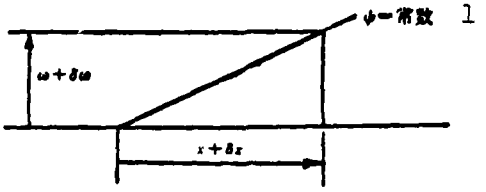

Figure 2. Diagram for Coordinate Transformation.
Key: 1. Constant.

Here the coordinate relationships between x, ψ, and ω are shown in Figure 2. From this we get the following equations

$$\left(\frac{\partial}{\partial x}\right)_\psi = \left(\frac{\partial}{\partial x}\right)_\omega + \left(\frac{\partial}{\partial \omega}\right)_x \left[\frac{-\frac{d\psi_1}{dx} - \omega \frac{d}{dx}(\psi_E - \psi_1)}{\psi_E - \psi_1}\right] \tag{16}$$

$$\left(\frac{\partial}{\partial \psi}\right)_x = \frac{1}{\psi_E - \psi_I}\left(\frac{\partial}{\partial \omega}\right)_x \tag{17}$$

where $\frac{d\psi_I}{dx} = -r_I \dot{m}_I''$, $\frac{d\psi_E}{dx} = -r_E \dot{m}_E''$

$\dot{m}_I''$ and $\dot{m}_E''$ represent the rate of mass transfer across the inner and outer boundary, respectively.

Using equations (16) and (17) we can transform the set of conservation equations (2'), (3'), and (4') into the following general form:

$$\frac{\partial \Phi}{\partial x} + (a + b\omega)\frac{\partial \Phi}{\partial \omega} = \frac{\partial}{\partial \omega}\left(c\frac{\partial \Phi}{\partial \omega}\right) + d \tag{18}$$

where $a = r_I \dot{m}_I''/(\psi_* - \psi_I)$

$b = (r_E \dot{m}_E'' - r_I \dot{m}_I'')/(\psi_E - \psi_I)$

$c = r^2 \rho u \mu_{eff}/[(\psi_E - \psi_I)^2 \sigma_{eff}]$

The source term, however, has different content which varies with the characteristic of the conservation equation[1].

Characteristic of the Equation	Variables	Content of term d
momentum equation	u	$-\frac{1}{\rho u}\frac{dp}{dx}$
mass transfer equation	m_j	$\frac{R_j}{(\rho u)}$
energy equation	h*	$\frac{\partial}{\partial \omega}\left\{\frac{r^2 \rho u \mu_{eff}}{(\psi_E - \psi_I)^2}\left(1 - \frac{1}{\sigma_{heff}}\right)\frac{\partial (u^2/2)}{\partial \omega}\right\}$

[1]The source term of the energy equation is derived after letting $\sigma_{Ieff} = \sigma_{heff}$.

Equation 18 is still a parabolic function and its numerical solution is obtained through the establishment of a difference equation described in the following section.

II. The Establishment and Solution of the Difference Equation

Let us take a finite controlled volume in the flow field as shown in Figure 3 and then carry out integration within the limits of the defined finite control volume to establish the difference equation. The use of this method to establish the difference equation has apparent advantages over the use of the Taylor series expansion method whether from the point of view of satisfying the physical concepts of the conservation equations or for the prevention of serious mathematical error[3].

Based on Appendix II, the difference equation is as follows:

$$g_1\Phi_{D^+} + g_2\Phi_D + g_3\Phi_{D^-} + g_4 = g_5(\Phi_{D^+} - \Phi_D) - g_6(\Phi_D - \Phi_{D^-}) + d_n + \left(\frac{\partial d}{\partial \Phi}\right)_n (\Phi_D - \Phi_n) \tag{19}$$

After simplification

$$\Phi_D = A\Phi_{D^+} + B\Phi_{D^-} + C \tag{20}$$

where

$$A = \frac{g_5 - g_1}{g_2 + g_5 + g_6 - (\partial d/\partial \Phi)_n}$$

$$B = \frac{g_6 - g_3}{g_2 + g_5 + g_6 - (\partial d/\partial \Phi)_n}$$

$$C = \frac{d_n - (\partial d/\partial \Phi)_n \Phi_n - g_4}{g_2 + g_5 + g_6 - (\partial d/\partial \Phi)_n}$$

For the conservation of momentum equation, due to the differ-

ent contents from treatment of the source term (see Appendix II), the difference equation corresponding to equation (20) is:

$$u_D = A_u u_{D^+} + B_u u_{D^-} + C_u \tag{21}$$

where

$$A_u = \frac{g_5 - g_1 + S_1}{g_2 + g_5 + g_6 - S_2}$$

$$B_u = \frac{g_6 - g_3 + S_3}{g_2 + g_5 + g_6 - S_2}$$

$$C_u = \frac{S_4 - g_4}{g_2 + g_5 + g_6 - S_2}$$

Based on the derivation in the Appendix it was found the equation (19) is the six point unexplicit difference form which has the characteristic of stability for any progressing steps.

The coefficients of the linear algebraic equations represented by equation (20) form a three diagonal linear matrix and solution can be found using an iterative method. For that equation (20) is simplified further as:

$$\Phi_i = A_i' \Phi_{i+1} + B_i' \tag{22}$$

where

$$A_i' = \frac{A_i}{1 - B_i A_{i-1}'}, \quad B_i' = \frac{B_i B_{i-1}' + C_i}{1 - B_i A_{i-1}'}, \quad A_1' = A_2, \quad B_2' = B_2 \Phi_1 + C_2$$

Because Φ_1 and Φ_{N+3} are determined by the boundary conditions, when the Φ_1 and Φ_{N+3} values are not given on the boundary, then their coefficients are zero. Here we theoretically solved the problem in seeking for a solution.

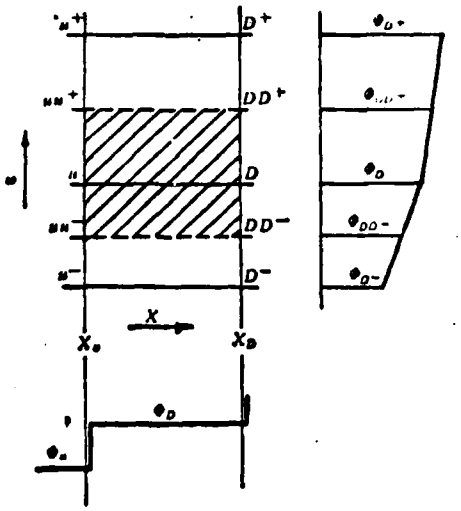

Figure 3. Controlled Volume

When the nodal points are chosen to be more dense, then the linear distribution of Φ value assumption in Figure 3 (On the Φ- ω plane) has already met the accuracy requirement for all the points in the flow field. But because the variation of Φ value is steeper near the boundary, if we still use the linear variation of the true value on the boundary, distortion will occur. Especially when the values of relative flux and transfer rate of a physical quantity on the boundary are to be determined, it would cause a large error. Because when these values are determined, it is necessary to use the gradient of Φ on the boundary and this gradient can not be replaced by the simply linear variation between the true Φ_1, value on the boundary and the Φ_3 value at its neighboring nodal point (refer to Figure 4). Therefore, during the process of solving for the the boundary layer problem, a sliding value problem on the boundary was proposed. That is it is possible to obtain the sliding value Φ_2 (or Φ_{n+2}) based on the distribution curve of Φ on various boundaries. The actual methods can be obtained by referring to Reference [2].

Because in the calculation of the sliding value we must consider the distribution of u on the boundary, therefore the shape of the distribution curve of u on the boundary would directly influence the accuracy of the results of computation of the boundary layer flow. Because the u value near the boundary is very small, from the set of conservation equations (2), (3), and (4) we can see that the convection along the x - axis can be neglected. This transforms and simplifies the flow near the boundary into the model of the Couette flow. Based on the characteristics of the Couette flow on the boundary, we can derive the value of u and the exponent of the distribution curve of the value of Φ.

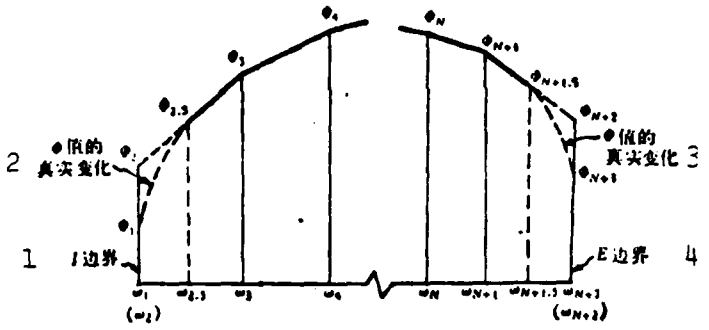

Figure 4. Definition of Sliding Value.
Key: I boundary, 2. True variation of Φ value, 3. True variation of Φ value, 4. E boundary.

Regarding the treatment of the source term $\frac{dp}{dx}$: For the flow with given $\frac{dp}{dx}$ distribution, we can directly use the above method to solve the problem. But for those problems with the distribution of $\frac{dp}{dx}$ yet to be determined in the flow process (such as the boundary layer flow problem in the restricted duct), it is relatively more complicated. Rigorously speaking, the value of the distribution of $\frac{dp}{dx}$ should be

resolved based on a iterative computation method. This requires to save all the parameters relevant to $\frac{dp}{dx}$ in the flow field and to carry out multiple iterations. This would significantly increase the computation time and memory units required which eliminates the advantages short time and few memory units necessary for the original progressing method used to obtain the solution to the parabolic equation. For that an approximation method is used.

The expression for $\frac{dp}{dx}$ can be derived based on the continuity equation and momentum equation of the one-dimensional flow as follows:

$$\frac{dp}{dx} = -\frac{F'}{A} - \frac{2\bar{u}}{A}\frac{d\dot{m}}{dx} + \frac{\dot{m}\bar{u}}{A}\left(\frac{1}{A}\frac{dA}{dx} + \frac{1}{\rho}\frac{d\rho}{dx}\right) \tag{23}$$

therefore

$$\frac{d\rho}{\rho} = \frac{dp}{p} - \frac{d\bar{T}}{\bar{T}}$$

$$\frac{dp}{dx} = \frac{-\frac{F'}{A} - \frac{2\bar{u}}{A}\frac{d\dot{m}}{dx} + \frac{\dot{m}\bar{u}}{A^2}\frac{dA}{dx} - \frac{\dot{m}\bar{u}}{A\bar{T}}\frac{d\bar{T}}{dx}}{1 - \frac{\dot{m}\bar{u}}{Ap}} \tag{24}$$

where

$$\bar{u} = \int r\rho u^2 dy \Big/ \int r\rho u dy, \quad \bar{T} = \int r\rho u T dy \Big/ \int r\rho u dy$$

For gas flow of low Mach number, the effect of pressure on density can be neglected. Thus the second term of the denominator on the right side of the equal sign no longer exists.

As for the physical meaning of $\frac{\dot{m}\bar{u}}{A^2}\frac{dA}{dx}$, it can be looked at as a discussion of a compressor flow problem. When the computation progressed to $x = x_0$, it was found that the results were that the fluid did not fill the entire cross-section of the compressor. This indicated that the original given $\frac{dp}{dx}$

value was incorrect. We should have started with a new assumption of $\frac{dp}{dx}$ to obtain the cross-section of the fluid until it finally matched the cross-section of the compressor. At the present moment this method is not used. Instead the computation proceeds to $x = x_D$. But the $\frac{dA}{dx}$ value which has an effect on the $\frac{dp}{dx}$ value is calculated using the following equation

$$\frac{dA}{dx} = \frac{(A_{d,D} - A_{f,a})}{x_D - x_a} \qquad (25)$$

This is to say that the difference in the $\frac{dp}{dx}$ value at the previous stop $(x = x_a)$ is partially compensated in the effect of area variation at the next stop $(x = x_D)$. In the actual calculation, a partial value of equation (25) should be used. Only by doing so that the instability of the calculated A_1 can be prevented.

In using the above method, it should be noticed that $A_{f,D}$ and $A_{d,D}$ must be very close at all times. They should be the same at some boundary points. Otherwise the approximation of the calculated flow field has no meaning whatsoever. (See Figure 5).

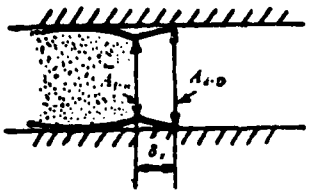

Figure 5. The physical meaning of dA/dx

As for the amount of partial value of equation (25) that should be used, it depends on the closeness of $A_{f,D}$ and $A_{d,D}$ which is checked during the computation process. For an approximate straight tube flow, we can use 0.1 - 0.2 as the correction

coefficient. For compressors which compress quickly, the correction coefficient is very small or is given by sections.

III. The Contents of the Computation Program and Computed Example

Computation program has been compiled based on the above discussion. Due to the limitation in pages, the block diagram and the actual content of the relevant program are omitted. The computer used to process the program was a Felix C-256 computer.

We have used this program to calculate a ring shaped compressor (Figure 6). With regard to the axial static pressure variation, the calculated and experimental values were compared and shown in the figure. The results are pretty close.

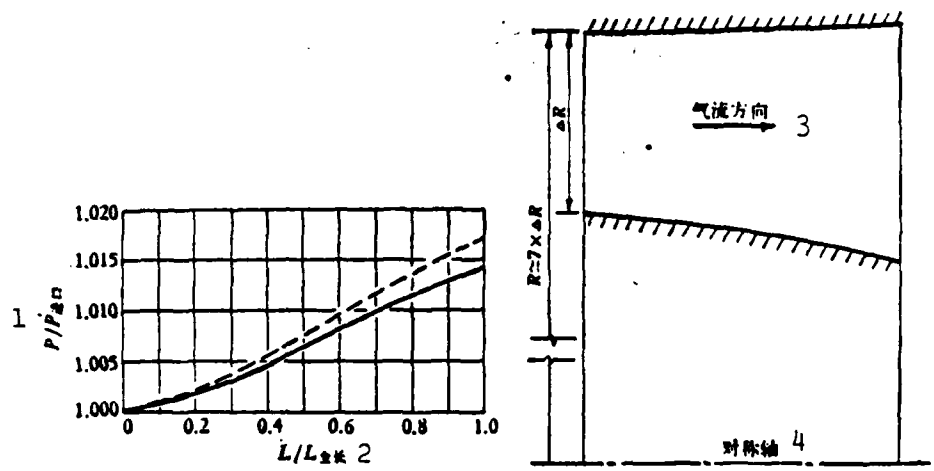

图6 计 算 实 例 8

—实验值 —计算值 (a) 扩压器沿轴向静压变化 7 (b) 环形扩压器几何图形 9

Figure 6. Computer Example. Key: 1. P/P inlet, 2. L/L total length, 3. direction of flow, 4. symmetry axis, 5. experimental value, 6. calculated value, 7. (a) axial static pressure variation of the compressor, 9. (b) geometric diagram of the ring shaped compressor.

IV. Closing Remarks

This paper based on the momentum equation expressed by stress tensor published in Reference [6] to derive the momentum equation of non-rotational steady axi-symmetric flow of a compressible fluid in the turbulent boundary layer in the axi-symmetrical coordinate system. It can be found very clearly from the derivation and discussion that equation (2') (similarly equations (3'), (4') and (18)) is not only suitable in solving the boundary layer problem on the surface of a revolved body but also applicable to the boundary layer problem of an axi-symmetric jet flow.

On the basis of Reference [2], the computer program after being partially modified by us can be applied to the following two situations from actual computational verification.

1. When the entire flow in the duct is treated by taking the viscosity into consideration, if the curvatore of the wall surface of the duct is not too large and the rate of curvature change in the direction of the flow is also not too large, then the entire flow field can be calculated based on this method.

2. If the curvature change of the duct is large then it is necessary to combine this method and the non-viscous flow in the main flow method to compute the solution.

Appendix I

The Deviation of the Continuity Equation and the Momentum Equation

When the compressible viscous fluid flows steadily in space, its continuity equation and momentum equation (without external force) are as follows:

$$\nabla \cdot (\rho V) = 0 \tag{I-1}$$

$$\nabla\left(\frac{1}{2}|V|^2\right) - V \times (\nabla \times V) = \frac{1}{\rho}\nabla \cdot \pi \tag{I-2}$$

Based on the vector and tensor operations introduced in Reference [6], for the non-rotational axi-symmetric flow in the axi-symmetrical coordinate system (Figure 1) considering that $k\delta$ and $\delta^2\left(\frac{dk}{dx}\right)$ are very small, then $h_1 = 1$, $h_2 = 1$, and $h_3 = r$. The coordinates corresponding to α, β, γ are x, y, θ. The components correspond to the vector quantity V are $v_1 = u$, $v_2 = v$, and $v_3 = 0$. In addition, all the variations in the θ direction for all the variables can be neglected[4].

Therefore, the continuity equation can be written as the following:

$$\frac{\partial}{\partial x}(\rho r u) + \frac{\partial}{\partial y}(\rho r v) = 0 \tag{1}$$

The equation of the x-direction momentum component is

$$\rho u \frac{\partial u}{\partial x} + \rho v \frac{\partial u}{\partial y} = \frac{\partial \pi_{xx}}{\partial x} + \frac{\partial \pi_{xy}}{\partial y} + \pi_{xx}\frac{\sin\vartheta}{r} + \pi_{xy}\frac{\cos\vartheta}{r} - \pi_{\theta\theta}\frac{\sin\vartheta}{r}$$

The relation between the stress tension π and the viscous stress tensor τ is as follows:

$$\tau_{ij} = \pi_{ij} + \delta_{ij}p$$

where δ_{ij} is the Kronecker δ, we get

$$\rho u \frac{\partial u}{\partial x} + \rho v \frac{\partial u}{\partial y} = -\frac{\partial p}{\partial x} + \frac{\partial \tau_{xx}}{\partial x} + \frac{\partial \tau_{xy}}{\partial y} + \frac{\tau_{xx}}{r}\frac{\sin\vartheta}{r} + \frac{\tau_{xy}}{r}\frac{\cos\vartheta}{r} - \frac{\tau_{\theta\theta}}{r}\frac{\sin\vartheta}{r}$$

Based on the qssumption made by Prandtl on the boundary layer, the above equation can be simplified into

$$\rho u \frac{\partial u}{\partial x} + \rho v \frac{\partial u}{\partial y} = \frac{\partial \tau_{xy}}{\partial y} + \frac{\cos\vartheta}{r}\tau_{xy} - \frac{\partial p}{\partial x} \tag{I-3}$$

After considering the effect of curvature, we can obtain the momentum component equation in the y equation as

$$\rho u' = \frac{1}{\rho} \frac{\partial p}{\partial y}$$

Therefore

$$\frac{1}{\rho} \frac{\partial p}{\partial y} = O(1)$$

Since the boundary layer belongs to the $O(\delta)$ class, the static pressure difference in the y direction in the actual boundary layer can be ignored.

Based on the conditions of the non-rotational axi-symmetrical flow and from an order of magnitude comparison, we know that the momentum component equation in the θ direction no longer exists.

For simplification, let τ represent τ_{xy} and also consider $\cos\vartheta = \frac{\partial r}{\partial y}$ and $\frac{\partial p}{\partial x} = \frac{dp}{dx}$ (because the static pressure difference in the y direction can be ignored). Equation (I-3) can then be transformed into the following:

$$\rho u \frac{\partial u}{\partial x} + \rho v \frac{\partial u}{\partial y} = \frac{\partial \tau}{\partial y} + \frac{\cos\vartheta}{r} \tau - \frac{dp}{dx} \qquad \text{(I-4)}$$

or

$$\rho u \frac{\partial u}{\partial x} + \rho v \frac{\partial u}{\partial y} = \frac{1}{r} \frac{\partial}{\partial y}(\tau r) - \frac{dp}{dx} \qquad (2)$$

As for the mass transfer equation (3) and energy equation (4), they can be derived using the same procedures as described above. It will not be repeated here.

Appendix II. The Principles Used in the Derivation of the Difference Equation

When establishing the difference equation, the relation between $\Phi-\omega$ and $\Phi-x$ used were linear and stair-case shaped distributions, respectively. As for the Φ value used in $\frac{\partial}{\partial\omega}$ the Φ value at the downstream x_D was used. This could insure the stability of the difference computation[2]. But the coefficient a, b, and c were obtained from the Φ value at x_μ upstream. The difference format of the equation was then established based on the integration with respect to the entire control volume for all the terms in equation (18).

The source term d has different content corresponding to different conservation equations. For mass transfer and energy conservation equations, we assumed that in the entire control volume the value of d was uniform and equal to the value d_D (i.e. $d-\omega$ or $d-x$ varies as a stair case shaped variation).

For the momentum conservation equation, the corresponding value of Φ is u. The calculated result of u would simultaneously influence the solutions to the mass transfer and the energy conservation equations. Therefore the importance of the more accurate assumption of the source term distribution in the momentum conservation equation becomes more apparent. Let us assume that the variation of $d-\omega$ between network nodal points was linear and the variation of d-x between the network nodal points was a staircase shaped variation.

Based on the above principles, we can derive the difference equation of the mass transfer or energy conservation equation

$$a_1\Phi_{D+} + a_2\Phi_D + a_3\Phi_{D-} + a_4 = a_1(\Phi_{D+} - \Phi_D) - a_3(\Phi_D - \Phi_{D-}) + d_* + \left(\frac{\partial d}{\partial \Phi}\right)_*(\Phi_D - \Phi_*) \qquad (19)$$

where

$$g_1 = \frac{1}{4}\frac{(\omega_{D+}-\omega_D)}{(x_D-x_a)(\omega_{D+}-\omega_{D-})} + \frac{a}{(\omega_{D+}-\omega_{D-})} + \frac{b}{4}\frac{(\omega_{D+}+3\omega_D)}{(\omega_{D+}-\omega_{D-})}$$

$$g_2 = \frac{3}{4(x_D-x_a)} - \frac{b}{4}$$

$$g_3 = \frac{1}{4}\frac{(\omega_D-\omega_{D-})}{(x_D-x_a)(\omega_{D+}-\omega_{D-})} - \frac{a}{(\omega_{D+}-\omega_{D-})} - \frac{b}{4}\frac{(\omega_{D-}+3\omega_D)}{(\omega_{D+}-\omega_{D-})}$$

$$g_4 = -\frac{1}{4}\frac{(\omega_{D+}-\omega_D)}{(x_D-x_a)(\omega_{D+}-\omega_{D-})}\Phi_{a+} - \frac{3}{4(x_D-x_a)}\Phi_a$$

$$-\frac{1}{4}\frac{(\omega_D-\omega_{D-})}{(x_D-x_a)(\omega_{D+}-\omega_{D-})}\Phi_{a-}$$

$$g_5 = \frac{2C_{aa+}}{(\omega_{D+}-\omega_{D-})(\omega_{D+}-\omega_D)}$$

$$g_6 = \frac{2C_{aa-}}{(\omega_{D+}-\omega_{D-})(\omega_D-\omega_{D-})}$$

Similarly, the difference equation of the corresponding momentum conservation equation can be derived

$$g_1 u_{D+} + g_2 u_D + g_3 u_{D-} + g_4 = g_5(u_{D+}-u_D) - g_6(u_D-u_{D-}) + S_1 u_{D+} + S_2 u_D + S_3 u_{D-} + S_4$$

where $g_1, g_2, g_3, g_4, g_5, g_6$ were defined as above, and

$$S_1 = \frac{1}{4\rho_{a+}u_{a+}^2}\left(\frac{dp}{dx}\right)_a\left(\frac{\omega_{D+}-\omega_D}{\omega_{D+}-\omega_{D-}}\right)$$

$$S_2 = \frac{3}{4\rho_a u_a^2}\left(\frac{dp}{dx}\right)_a$$

$$S_3 = \frac{1}{4\rho_{a-}u_{a-}^2}\left(\frac{dp}{dx}\right)_a\left(\frac{\omega_D-\omega_{D-}}{\omega_{D+}-\omega_{D-}}\right)$$

$$S_4 = -\frac{1}{2}\left(\frac{dp}{dx}\right)_a\left[\frac{1}{\rho_{a+}u_{a+}}\left(\frac{\omega_{D+}-\omega_D}{\omega_{D+}-\omega_{D-}}\right) + \frac{3}{\rho_a u_a}\right.$$

$$\left. + \frac{1}{\rho_{a-}u_{a-}}\left(\frac{\omega_D-\omega_{D-}}{\omega_{D+}-\omega_{D-}}\right)\right]$$

References

[1] Gosman, A. D., Pun, W. M., Runchal, A. K., Spalding, D. B., Wolfshtein, M., Heat and Mass Transfer in Recirculating Flows, Academic Press (1969).

[2] Patankar, S. V., Spalding, D. B., Heat and Mass Transfer in Boundary Layers, Intertext Books (1970).

[3] Spalding, D. B., A General Computer Program for Two-Dimensional Boundary-Layer Problems, Imperial College of Science and Technology, Department of Mechanical Engineering (1973).

[4] Goldstein, S., Modern Developments in Fluid Dynamics, Oxford University Press (1938), 128—130.

[5] Mangler, W., Zusammenhang zwischen ebenen und rotationssymmetrischen Grenzschichten in Kompressiblen Flüssigkeiten, ZAMM, 28(1948), 97—103.

[6] Chien, T.S. "Equations in Gas Dynamics", Science Publication (1966), 58-60.

Abstract

A momentum equation of steady two-dimensional axi-symmetrical turbulent boundary layer is derived employing stress tensor analysis. It is found that if the flow in a duct is to be treated as viscous everywhere, the equation is valid only if the curvature of the duct and the rate of change of the curvature of the duct in the flow direction are small. These requirements so far have not been verified by previous authors.

In this paper, a computer program for solving the governing equations has been completed and a numerical example is selected to show its degree of accuracy.

LAMINAR HEAT TRANSFER WITH MASS INJECTION AND CHEMICAL REACTION

Zu Tie-lin[1]

In order to simplify the boundary layer problem with mass injection and chemical reaction, a general stoichiometric formula has been derived. Using the chemical equilibrium as an example we performed an analysis. The calculated results were found to be consistent with the experimental ones. When the amount of injection is zero, the relevant data were in good agreement with the results listed in Reference [4]. Finally, it was pointed out that with the increasing available energy of the exothermic reaction the effect of Lewis number Le on the heat transfer decreases.

In the boundary layer problem with mass injection and chemical reaction, one usually assumes that the Lewis number Le = 1 in the combustion loss calculation in order to obtain relatively simple results. Along with increasing amount of injection and variation of other relevant conditions, this assumption would cause significant errors in the results of calculated heat transfer and effective combustion heat. Lees[1] has provided an analytical solution for Le ≠ 1 which is expressed by Blasius function to the wall surface chemical equilibrium problem of a frozen boundary layer with a constant transfer characteristic. This paper studied the affect of chemical reaction on the heat transfer through a discussion of a chemical equilibrium boundary layer with Le ≠ 1. We have carried out a

This paper was received on December 9, 1977.

1 This paper was written in 1964 during the period when the author was working at Institute of Mechanics of Chinese Science Academy. It was presented in the Combustion Technology Meeting at Daireu in 1964. The author's present place of employment: Central Weather Bureau, Institute of meterology research, atmospheric weather research department.

discussion on the equations of boundary layer chemical reaction and wall surface conditions and obtained an universal generalized stoichiometric formula. Using the assumption imposed by Lees, we provided the numerical solution to a series of examples for the equilibrium boundary layer. After further making a linearity assumption, we obtained an approximate equilibrium solution similar to Lees' frozen solution.

In the constant transfer assumption, the most worthwhile discussing subject is the applicability of using Fisk's Law to express the mass flow and taking Le as a constant. The author has written an article on this subject with Yao Kang-Chun and Hu Cheng-Hwa in 1964 (unpublished). That paper compared the heat transfer calculated in the decomposition of air using the multiple element method and the two-element method with a constant Le number. Its conclusion was that when the constant Le number was properly chosen we could obtain the same heat transfer as the one calculated by the multiple element method. (Figure 1). As for the combustion reactions in decomposed air, as long as a proper Le number is chosen, we will get the same result.

I. Basic Equations and Generalized Stoichiometric Formula

The continuity, diffusion, momentum and energy (expressed by the frozen enthalpy H_T)equations of a steady laminar boundary layer with chemical reaction are:

$$(\rho u r^{\nu})_x + (\rho v r^{\nu})_y = 0 \tag{1}$$

$$\rho u K_{i,x} + \rho v K_{i,y} = -J_{i,y} + \omega_i \quad (i = 1, 2, \cdots, l) \tag{2}$$

$$\rho u u_x + \rho v u_y = -P_x + (\mu u_y)_y \tag{3}$$

$$\rho u H_{Tx} + \rho v H_{Ty} = \left[\frac{k}{\bar{c}_p} H_{Ty}\right]_y + \left[\mu\left(1 - \frac{1}{Pr}\right)\left(\frac{u^2}{2}\right)_y\right]_y \qquad (4)$$
$$- \left[\sum_{i=1}^{I} J_i h_i\right]_y - \left[\frac{k}{\bar{c}_p} \sum_{i=1}^{I} h_i K_{iy}\right]_y - \sum_{i=1}^{I} \omega_i h_i$$

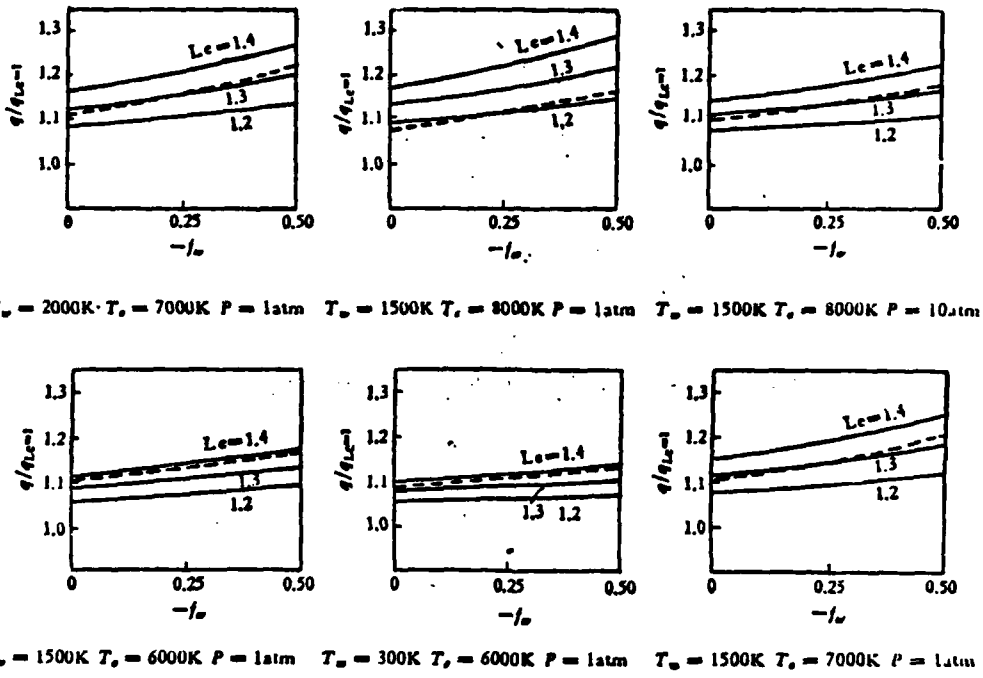

Figure 1. Heat Transfer Calculated Using the Multiple Element Method and Two-Element Method. Key: 2. Multiple element method, 3. Two-element method. ---多组元 (2) ——二组元 (3)

Where r is the radius of the revoluted body; when $\varepsilon = 0$ it is a two dimensional flow; When $\varepsilon = 1$, it is a three dimensional axi-symmetrical flow; ρ is the density of the mass; u and v are respectively the velocity components in the x and y direction; x and y are respectively coordinates along the direction of the object and that perpendicular to the surface of the object; the subscript i represents any element in the complete element 1; K is the concentration (mass ratio); J is the mass flow; ω is the chemical rate of formation; P is the

pressure; μ is the viscosity; the frozen enthalpy $H_T = h + \frac{u^2}{2}$, $h = \sum_{i=1}^{I} K_i h_i$, $h_i = \int_0^T c_{pi} dT$; c_{pi} is the isobaric specific heat of element i; the isobaric specific heat of the gas mixture $\bar{c}_p = \sum_{i=1}^{I} K_i c_{pi}$; K is the thermal conductivity; the Praneltl number Pr = $\frac{\bar{c}_p \mu}{k}$; h_i^0 is the enthalpy of formation at 0°K for a unit mass of element i.

Let us assume that every element is a perfect gas, then

$$P_i M_i = \rho_i RT \tag{5}$$

$$P\bar{M} = \rho RT \tag{6}$$

When $\bar{M} = \left(\sum_i K_i \frac{1}{M_i}\right)^{-1}$, and M_i is the molecular weight of the element i; R is the conventional gas constant. Let us assume that the mass flow can be expressed using Fisk's Law, which treats the diffusion coefficients D_{ij} of the two elements the same (both to be D) and only considers concentration diffusion, then

$$J_i = -\rho D K_i, \tag{7}$$

When ω_i is frozen at zero and it is a function of the local p, T, and K_i when there is chemical reaction. The functional relation is given by the chemical kinetic conditions. Let us assume that there are a total number of s independent chemical reactions in the problem we are considering:

$$\sum_{i=1}^{I} n_i^p X_i = 0 \quad (p = 1, 2, \cdots, s) \tag{8}$$

where n_i^p is the stiochiometric coefficient of element i in the pth chemical reaction; X_i is the molecular formula of element i. Every reaction in equation (8) has only one independent reaction rate. s is usually smaller than 1. In order to solve for the mass ratio of the entire 1 elements, the 1 - s diffusion

equations necessary to be preserved are usually transformed into the frozen form using the conservation of element method. This method is mandatory for equilibrium problems. For non-equilibrium problems, the calculation procedure can be simplified and it is irrelevant whether the mass flow is expressed using equation (7). In order to overcome the disadvantages of using the conservation of element method such as the inconvenience to put it into a routine form and inability to choose the reference element, this paper obtained a "generalized stoichiometric formula."

Let us make the reaction rates of l - s elements out of the l elements in the l - s reactions $\omega_1^j, \omega_2^j, \cdots, \omega_l^j$ to be independent, then the rate of formation of each element can directly be expressed by the linear combination of the s independent rates of formation:

$$\omega_i = \sum_{j=s-1}^{l} \alpha_i^j \omega_j^p \quad (i = 1, 2, \cdots, l) \tag{9}$$

where

$$\alpha_i^j = \frac{(n_i^p M_i)}{(n_j^p M_j)} \tag{10}$$

If we consider the problem as a linear space problem, then this set of independent rates of formation can be mathematically treated as a set of independent vectors of a "basis". The coefficient a_1^j then becomes the coordinate under this "basis". The ω_j^p appearing in equation (9) is not convenient to use, it is necessary to select a new "basis" $(\omega_1, \omega_2, \cdots, \omega_s)$, which is expressed by the total reaction rate. The reaction rate not included in the new "basis" or the non-independent reaction rate can be expressed linearly using the new "basis":

$$\omega_k = \sum_{i=s-1}^{l} \chi_k^i \omega_i \quad (k = s+1, s+2, \cdots, l) \tag{11}$$

where

$$\begin{pmatrix} \chi_k^1 \\ \vdots \\ \chi_k^l \end{pmatrix} - \begin{pmatrix} a_1^1 \cdots a_s^1 \\ \vdots \quad \vdots \\ a_1^l \cdots a_s^l \end{pmatrix}^{-1} \begin{pmatrix} a_k^1 \\ \vdots \\ a_k^l \end{pmatrix} \tag{12}$$

Equation (11) is the generalized stoichiometric formula. The use of this formula is especially convenient for problems with complicated chemical reactions. Let us define the symbol:

$$\mathscr{L} = \rho u \frac{\partial}{\partial x} + \rho v \frac{\partial}{\partial y} - \frac{\partial}{\partial y}\left(D\rho \frac{\partial}{\partial y}\right) \tag{13}$$

and then equation (2) can be written as:

$$\mathscr{L} K_i = \omega_i \tag{14}$$

Substituting equation (14) in equation (11), we get

$$\mathscr{L} \tilde{R}_k = 0 \tag{15}$$

$$\tilde{R}_k = K_k - \sum_{i=1}^{s} \chi_k^i K_i \quad (k = s+1, \cdots, l) \tag{16}$$

Equation (15) is the preserved (1 - s) diffusion equations in the frozen form. The remaining s equations are provided by the s chemical reaction conditions. When the chemical reactions are in equilibrium, the s conditions are

$$\prod_{i=1}^{l} \left(\frac{K_i}{M_i}\right)^{a_i^p} (P\bar{M})^{\sum_{i=1}^{l} a_i^p} = \mathscr{K}_p \tag{17}$$

where $\mathscr{K}_p$ is the balancing constant of the p^{th} reaction. If we slightly change the operating symbol $\mathscr{L}$ by substituting ω_i with the rate of formation per unit area m_i, then equation (15) can be expanded to the boundary or any plane.

II. Approximate Solution and Iteration Equations

Let us consider $Pr, Le\,(=\rho D\bar{c}_p/k), l\,(=\rho\mu/\rho_w\mu_w)$ to be reference constants. For practical reasons, let us limit our discussion to the point of the revoluted body. The following type of correction was made using the Mangler-Dorodonitsyn transformation:

$$\left.\begin{aligned}\eta &= \frac{ru_e\rho_w\mu_w}{2\sqrt{\xi}}\int_0^y \frac{\bar{c}_p}{k}\,dy\\ \xi &= \int_0^x \rho_w\mu_w u_e r^2\,dx\end{aligned}\right\} \tag{18}$$

where the subscripts e and w represent the wall surface and outer fringe of the boundary layer values, respectively. Let us define the following dimensionless quantities:

$$f_\eta = 2\frac{u}{u_e},\quad g_T = \frac{H_T}{H_{T_0}} = \int_0^T \bar{c}_p\,dT \Big/ \int_0^{T_0} \bar{c}_p\,dT.$$

For cold walls, we can neglect the pressure gradient term in the momentum equation.[3] Let us assume that the C_{pi} for every element is the same and use equation (11) in the energy equation, then the basic equations can be written as

$$f_{\eta\eta\eta} + ff_{\eta\eta} = 0 \tag{19}$$

$$\tilde{K}_{k\eta\eta} + Scf\tilde{K}_{k\eta} = 0 \quad (k = s+1, s+2, \cdots, l) \tag{20}$$

$$\left(g_T + Le\sum_{j=1}^{s} h'_{ik}K_j\right)_{\eta\eta} + Prf\left(g_T + Le\sum_{j=1}^{s} h'_{ik}K_j\right)_\eta - Prf(Le-1)\sum_{j=1}^{s} h'_{ik}K_{j\eta} \tag{21}$$

where $Sc = Pr/Le,\ \tilde{h}'_{ik} = h'_{ik}/H_{T_0},\ h'_{ik} = h^0_i + \sum_k \chi_k h^0_k$. The boundary

conditions for these equations are:

$$\left.\begin{aligned} &f_\eta(0) = 0,\ f(0) = f_w = -(\rho v)_w/(r^{-1}\xi^{-\frac{1}{2}}\xi_e l^{\frac{1}{2}}) \\ &f_\eta(\infty) = 2 \\ &\tilde{K}_i(0) = \tilde{K}_{iw},\ \tilde{K}_i(\infty) = \tilde{K}_{ie} \\ &g_T(0) = g_{Tw},\ g_T(\infty) = 1 \end{aligned}\right\} \tag{22}$$

As for the s equations lacking in finding solutions to K_i, equation (17) will be used as the supplement for equilibrium problems.

We carried out integration for equations (20) and (21) and wrote the result of integration of equation (21) in an iterative form. We get

$$\tilde{K}_i - \tilde{K}_{iw} = (\tilde{K}_{ie} - \tilde{K}_{iw})\beta(\eta; f_w, \mathrm{Sc}) \tag{23}$$

$$\tilde{K}_{i\eta w} = (\tilde{K}_{ie} - \tilde{K}_{iw})\beta_\eta(0; f_w, \mathrm{Sc}) \tag{24}$$

$$\begin{aligned}(g_T + \mathrm{Le}\bar{h}_{ch})^{(n)} - (g_T + \mathrm{Le}\bar{h}_{ch})_w = \{&g_{Te} - g_{Tw} + [\mathrm{Le} - (\mathrm{Le}-1)G^{(n-1)}(\infty)] \\ &\cdot (\bar{h}_{che} - \bar{h}_{chw})\}\beta(\eta; f_w, \mathrm{Pr}) + G^{(n-1)}(\eta)\end{aligned} \tag{25}$$

$$\begin{aligned}(g_T + \mathrm{Le}\bar{h}_{ch})^{(n)}_{\eta w} = \{&g_{Te} - g_{Tw} + [\mathrm{Le} - (\mathrm{Le}-1)G^{(n-1)}(\infty)](\bar{h}_{che} - \bar{h}_{chw})\} \\ &\cdot \beta_\eta(0; f_w, \mathrm{Pr})\end{aligned} \tag{26}$$

where β is the Blasius function:

$$\beta(\eta; f_w, z) = \int_0^\eta f_\eta^2 d\eta \Big/ \int_0^\infty f_\eta^2 d\eta \tag{27}$$

z = Sc or Pr. The detailed numerical table of β and β_η is given in Reference [2].

$$\bar{h}_{ch} = \sum_{i=1}^{s} \bar{h}^i_{ch} K_i$$

$$G(\eta) = (\bar{h}_{che} - \bar{h}_{chw})^{-1} \sum_{i=1}^{s} \bar{h}^i_{ch}(K_{ie} - K_{iw})G_i(\eta) \tag{28}$$

$$G_i(\eta) = (K_{ie} - K_{iw})^{-1}\mathrm{Pr}\int_0^\infty e^{-\mathrm{Pr}\int f d\eta}\int_0^\eta f e^{\mathrm{Pr}\int f d\eta} K_{i\eta} d\eta d\eta \tag{29}$$

Under the situation that the boundary conditions are known, equation (26) can provide the heat transfer which we are interested in obtaining. The $G(\infty)$ in the equation usually has to be obtained through the iteration equation set (23) - (29) and equation (17). The first order approximation of $G(\infty)$ can be calculated using the $K_{i\eta}$ when Le = 1. Calculation makes clear that convegence in this form of equation is very quick.

When the temperature in the boundary layer exceeds 2000°K, because the vibrational degrees of freedom for every element are nearly all excited, $\bar{C}_p$ can be treated approximately as a constant. At this time in equations (25) and (26) $g_T = \theta = T/T_e$. It is even simpler to find the solution.

III. Wall Surface Mass Ratio and Heat Transfer

By integrating equation (20) from $\eta = 0$ to $\eta = 0 + \varepsilon$ (ε is a small quantity) and also noticing equation (24), we can obtain the conservation of mass conditions of wall surface

$$\tilde{K}_{iw} = (\tilde{K}_{iw-}B + \tilde{K}_{iw})/(B + 1) \tag{30}$$

where $\tilde{K}_i$ is defined by equation (16); K_{iw} - represents the mass ratio before injection (i = K or j), for non-injection elements $K_{iw-} = 0$; and K_{iw} represents the mass ratio after the injection and chemical reaction.

$$B = -\frac{Sc f_w}{[\beta_1(0; Sc, f_w)]} \tag{31}$$

Using wall temperature as a parameter, equation (30) and equation (17) (or general catalytic conditions) form a set of closed equations within which K_{iw} can be solved.

With different mass injection conditions, we can divide the wall surface onto three types of problems and they

are the "homogeneous reaction", the "heterogeneous reaction", and the combination of the two above. For "heterogeneous reaction" (such as the combustion of carbon), the quantity B of interest in the combustion loss calculation can be directly solved using the above method. This is because the K_{iw} of the solid phase element is always 1 in equation (17) and it is 0 in equation (30). For "homogeneous reaction", the mass ratio before injection should be given by the condition in the wall (material composition, control method, etc.).

Using the approximation method to integrate the energy equation (21) near the wall surface, we can get the heat transfer into the wall as

$$q_w = k\frac{\partial T}{\partial y}_{w-} = \beta_s(0; f_w, \mathrm{Pr}) l^{\frac{1}{2}} \mathrm{Pr}^{-n} \times \sqrt{\rho_w \mu_w \left(\frac{du_s}{dx}\right)_s} (H_{Te} - H_{Tw} + \mathrm{Le}^r \Delta h_{ch} - B\,\mathrm{Le}^{r\gamma} L_E) \tag{32}$$

where

$$\Delta h_{ch} = \sum_{i=1}^{i} \{K_{ie} - [(B+1)K_{iw} - BK_{iw-}]\} h_{ch}^i \tag{33}$$

$$\mathrm{Le}^r = 1 + (\mathrm{Le} - 1)[(1 - G(\infty)) + H_s(G(\infty) - G_f(\infty))] \tag{34}$$

$$\gamma \approx 1 - G(\infty) + H_s[G(\infty) - G_f(\infty)] \tag{35}$$

The latent heat of phase change is $L_E = H_{TW} - H_{TW-}$. The subscript f represents the frozen value. When frozen, $G(\infty) = G_f(\infty)$, $\mathrm{Le}^r \to \mathrm{Le}^{r_f}$, $\gamma_f \approx 1 - G_f(\infty)$. γ_f was given in Reference [1]. The subscript s represents the stationary point value.

If we neglect the differences of parameters such as Pr, Le, l, etc. between the equilibrium and frozen conditions, from equation (32) we can see that the exponent γ is the only para-

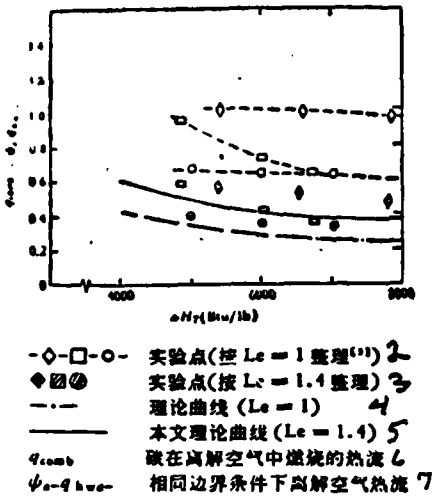

igure 2. Comparison of Theoretical and Experimental Results Key: 2. Experimental points (arranged based on Le = 1[5]), 3. Experimental points (arranged based on Le - 1.4), 4. Theoretical curve (Le = 1), 5. Theoretical curve derived in this work (Le = 1.4), 6. Heat transfer of carbon combustion in decomposed air, 7. Heat transfer of decomposed air under same boundary conditions.

meter to indicate the effect of chemical kinetic condition in the boundary layer on the heat transfer. Similar to the kinetic energy recovery factor which depends on the Pr number, Le^r here corresponds to the extent of the transformation of the excess chemical enthalpy of the outer fringe compared to the wall surface into thermal enthalpy. Because the generalized stiochiometric formula used can arbitrarily choose the reference element, it is very convenient to select the element with concentration at the wall surface to be zero (not zero in the outer fringe) as the reference element in the calculation of equations (32) - (35).

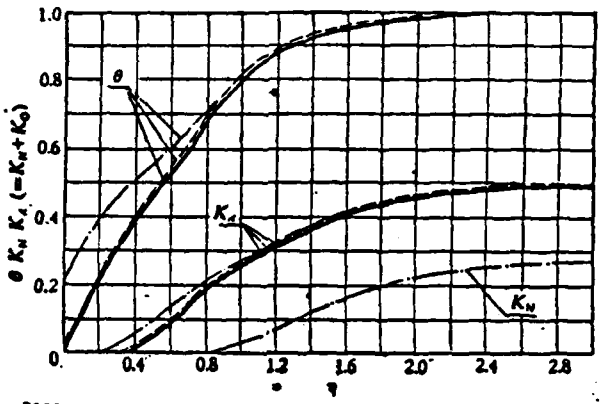

$T_e = 7000K$ $P = 3.5atm$ $f_\infty = 0$ $Le = 1.4$ $Pr = 0.71$ 壁面反应平衡 2
—·— $T_\infty = 1500K$ [本文]3 – – – $T_\infty = 300K$ [4] ——$T_\infty = 300K$ [本文] 4

Figure 3. The distributions of the dimensionless temperature θ and the nitrogen and oxygen atomic mass ratios along η in the equilibrium boundary layer of decomposed air.
Key: 2. wall surface reaction equilibrium, 3. this work, 4. this work.

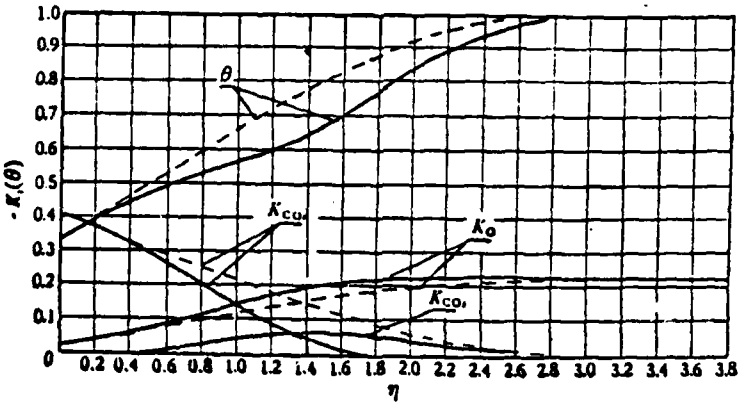

$T_e = 6000K$ $T_\infty = 2000K$ $P = 3.5atm$ $-f_\infty = 0.25$ $Le = 1.2$ $Pr = 0.71$ 壁面反应 2
3 平衡 边界层内反应为 $CO + O = CO_2$ (假设氮不离解,氧不过合)
4 —— 平衡分布 5 —— 冻结分布

Figure 4. The distributions of the dimensionless temperature θ and the mass ratio $K_i (i = CO_2, CO, O)$ along η in the combustion of carbon monoxide. $T_e = 6000K$ $T_\infty = 2000K$ $P = 3.5atm$ $-f_\infty = 0.25$ $Le = 1.2$ $Pr = 0.71$
Key: 2. wall surface reaction, 3. equilibrium: the reaction in the boundary layer is $CO + O = CO_2$ (assuming nitrogen does not recombine), 4. equilibrium distribution, 5. frozen distribution.

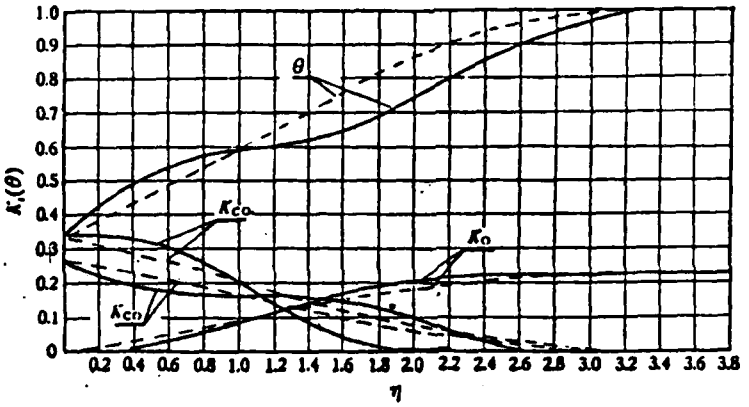

Figure 5. The distributions of the dimensionless temperature θ and mass ratio $K_i(i = CO_2, CO, O)$ along η in the combustion of carbon monoxide. $T_e = 6000K$ $T_w = 2000K$ $P = 3.5atm$ $-f_w = 0.5$ $Le = 1.2$ $Pr = 0.71$

Key: 7. Wall surface reaction equilibrium: the reaction in the boundary layer is $CO + O = CO_2$ (assuming nitrogen does not decompose and oxygen does not recombine), 8. equilibrium distribution, 9. frozen distribution.

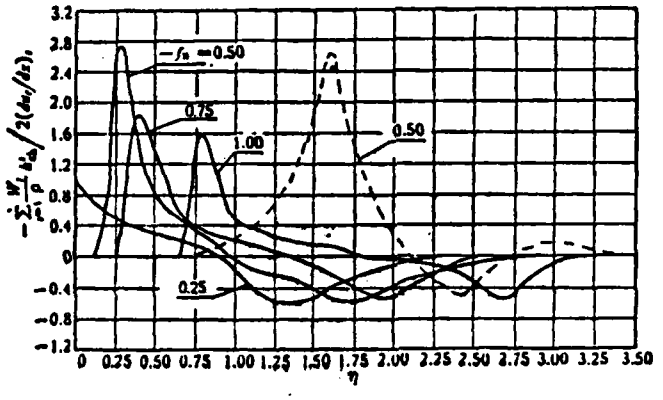

Figure 6. The distribution of the dimensionless total heat of reaction $-\sum_{i=1}^{5} \frac{\omega_i}{\rho} H_{i_0} / 2\left(\frac{du_e}{dx}\right)_e$ along η.

Key: 11. example 3, 12. example 4.

This paper conducted heat transfer calculations for the following examples. 1) The homogeneous injection of air, the reaction equation is $O_2 \rightleftharpoons 2O$, $N_2 \rightleftharpoons 2N$; 2) the homogeneous injection of oxygen, which is the injection of oxygen in an scattered flow of oxygen, the reaction equation is $O_2 \rightleftharpoons 2O$; 3) the homogeneous injection of nitrogen, the reaction equation is $N_2 \rightleftharpoons 2N$; 4) the injection of carbon monoxide, the reaction equation is $CO + O \rightleftharpoons CO_2$; 5) the injection of carbon monoxide, the reaction equations are $CO + O \rightleftharpoons CO_2$, $2O \rightleftharpoons O_2$; 6) the injection of carbon monoxide, the reaction equations are $\rightleftharpoons CO_2$, $2O \rightleftharpoons O_2$, $2N \rightleftharpoons N_2$. The results of example 1 at zero injection agreed with the results of Reference [4] very well. In Reference [5], they have found that the theoretical results obtained by taking Le = 1 was far different from the results they obtained from their carbon combustion experiment. If the original data in Reference [5] were rearranged using the method described in this paper and let Le = 1.4, then it was found that all the experimental points were located either above or below the theoretical values obtained using this method (see Figure 2). Figures 3 - 6 provided the distributions of K_1, T, $-\sum_{i=1}^{i} \frac{\omega_i}{\rho} \bar{h}_{ch} \Big/ 2\left(\frac{du_e}{dx}\right)_e^*$ along η. Figures 7 - 8 showed the variations of f_w, T_e, and T_w with γ. The two extrema in the distribution of $-\sum_{i=1}^{i} \frac{\omega_i}{\rho} \bar{h}_{ch} \Big/ 2\left(\frac{du_e}{dx}\right)_e$ along η correspond to the maximum exothermic and endothermic surfaces.

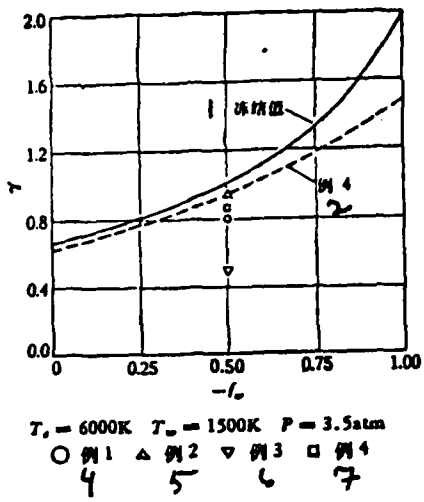

Figure 7. The variation of the chemical kinetic parameter γ with $-f_w$.
Key: 1. frozen value, 2. example 4, 4. example 1, 5. example 2, 6. example 3, 7. example 4, 8. example 1, 9. example 2, 10. example 3.

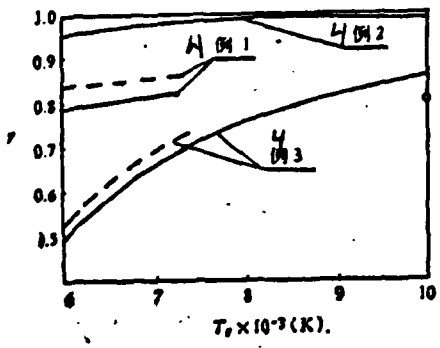

Figure 8. The variation of the chemical kinetic parameter γ with the outer fringe temperature T_e.
Key: 4. example
$(-f_w = 0.5)$
—T_w = 1500K, —T_w = 2000K } P = 3.5atm
○ T_w = 1500K P = 2.5atm

IV. The Approximate Solution and Discussion

When Le is not too far away from 1, we can expand K_i and g_T around (Le - 1) and obtain:

$$K_i = K_i^{(0)} + (Le-1)K_i^{(1)} + O[(Le-1)^2] \tag{36}$$

$$g_T = g_T^{(0)} + (Le-1)g_T^{(1)} + O[(Le-1)^2] \tag{37}$$

Let us neglect all the small terms after the second order term of (Le - 1), then G(∞) can be solved from the energy equation with Le = 1. From equation (21) it was found that the assumptions that all C_{pi} are identical and that $\frac{h_i}{h} - 1$ (or $\frac{c_{pi}}{\bar{c}_p} - 1$) and Le - 1 are small quantities of the same order of magnitude are equivalent. The concentration of the selected reference element at the wall surface is zero. When $\eta_1 > \eta > 0$ and $\eta_3 < \eta < \eta_\delta$ ($\eta_3 > \eta_1, \eta_\delta$ is the value of η at β = 0.99), $K_{i\eta} \to 0$ and K_j is monoclinic in the region $\eta_1 < \eta < \eta_3$. At this time, $H_\delta = 0$, Le^r has the same expression as in the frozen state:

$$Le^r = 1 + (Le-1)(1-G)$$

or

$$\gamma \approx 1 - G$$

Let us rewrite $K_{j\eta}$ into $K_{i\eta} = K_{i\infty} S_{i\delta} \bar{\theta}_\eta$. Where $S_i = K_i/K_{i\infty}$, $\bar{\theta} = (\theta - \theta_1)/(\theta_2 - \theta_1)$, and θ_1 and θ_2 are the dimensionless temperatures corresponding to η_1 and η_2, respectively. Let us assume that $S_{i\delta} = 1$. This assumption is suitable for the air decomposition problem when the pressure is not too high. For other combustion reactions, it corresponds to an assumption that reaction only takes place at η_1 and η_2 (corresponding to the maximum exothermic and endothermic surfaces in Figure 6). Assuming Pr = 1 and using the subscripts 1 and 2 to respectively represent the values at η_1 and η_2, we obtain the following by integrating G_j between the

regions η_1 to η_2:

$$G_j = \left[\ln\frac{(f_{\eta\eta})_2}{(f_{\eta\eta})_1} + \frac{1}{4}(f_1^2 - f_2^2)\right]/(\beta_{j2} - \beta_{j1}) \qquad (38)$$

Based on the reaction initiation and termination conditions of the reference element at η_1 and η_2, the η value is determined using the method of determination of the boundary layer thickness. Furthermore, through Le = 1 and using the energy equation with constant $\bar{c}_p$ as well as equation (17), β_{j1} and β_{j2} can be solved. From here we can locate the corresponding $f_{\eta\eta}$ and f from the Blasius table. The calculation indicates that the error is less than 5% comparing the γ value obtained using the approximation method used in this section with the calculated results obtained in the last section.

When $\beta_{j1} \to 0$, $\beta_{j2} \to 1$, $G_j \to G_j$ (G_j is consistent with the results in Reference [1]). When $\beta_{j2} \to 1$, and $\beta_{j1} \to 1$ also, $G_j \to 1$, and $\gamma_j \to 0$. This corresponds to the overlapping of two reaction surfaces at the outer fringe. Similar to the turbulent layer, a concentration type of discontinuity appears at the outer fringe. The transfer process has no effect on the heat transfer. In reality, situation can only exist close to that condition. For example, when T_e = 6000 K (cold wall condition) the η_1 of nitrogen is very close to the outer fringe. It is meaningful to have identical results when G_1 = 1 and Le = 1. If we define the extent of exothermic reaction occurring in a relatively high temperature region as the reactivity, then the assumption that Le = 1 is only suitable for problems with strong reactivity. When $\beta_{j1} \to 0$ and $\beta_{j2} \to 0$ also, we can get $G_j = f_w/\beta_{\eta}(0; f_w)$. This corresponds to the situation that the concentration interruption surface is right on the wall surface. When the injection quantity is constant, the γ value is maximum at this time which also means that at this time the effect of the transfer process has the most effect on the heat transfer. When the

pressure is lower and the temperature of the outer fringe is higher, the oxygen decomposition reaction is approximately in this situation. Corresponding to the -fw value of 0.25, 0.50, 0.75 and 1.00, the value of $G_j = f_w/\beta_{jw}(0;f_w)$ are 0, -0.51, -1.52, -4.0, and -14.1, respectively; and the corresponding γ_j are 1.53, 1.84, 2.34, 3.33, and 6.55 times the frozen value γ_{jf}, respectively. This explains that when there is chemical reaction going on, γ may also be greater than γ_f.

When $0<-f_w<0.5$ using β_{j1} and β_{j2} as variables we can linearly expand G_j around the two points $\beta_{j1} = 0$ and $\beta_{j2} = 1$ to get

$$G_j = G_j + \left[G_j - \frac{f_w}{\beta_{jw}}\right]\beta_{j1} + (1 - G_j)(\beta_{j2} - 1) \qquad (39)$$

In the above equation, because G_f is less than 1 and also less than $|f_w|$ and f_w is always negative in injection problems, the coefficients of β_{j1} and β_{j2} are always positive. Therefore, G_j increases with increasing β_{j1} and β_{j2} and γ_j decreases with increasing β_{j1} and β_{j2}. This explains that: when the reactivity is stronger or the reaction surface is closer to the higher temperature outer fringe, the effect of the transfer process on the heat transfer is weaker. All the factors which can increase the reactivity such as reactions with high equilibrium constants, increasing the injection quantity of the reactant, decreasing temperature for a fixed reaction, increasing the pressure, etc. can make γ_j smaller (refer to Figures 7 - 8).

For problems containing two or more reactions, we should still calculate the contribution to the total enthalpy change from the enthalpy difference $(K_w - K_{iw})\bar{h}_{ih}$ for each reaction based on equation (28). The higher the enthalpy difference the more its recovery capability contributes to the total recovery capability Le^{γ}. Since the mass ratio and enthalpy of formation

of nitrogen far exceeds those of oxygen in air, the γ of decomposed air with chemical reaction is usually smaller than γ_f when the outer fringe temperature is sufficiently high. With increasing outer fringe temperature, other reactions taking place in the decomposed air would further promote the deviation of γ in the less than γ_f direction. The combustion reactions in decomposed air are merely reactions between the combustible material with the relevant elements in air. The trend of variation of γ is similar to that of the above discussed pure decomposed air problem.

V. Conclusions

Using the generalized stoichiometric formula (11) to eliminate the non-independent reaction rates has the convenience of arbitrary selection of a reference element. This method is more routine than any other methods. Therefore, it is more suitable for problems with complicated chemical reactions.

The heat transfer can be calculated using the set of given iteration equations. Calculation and analysis both indicate that: the increase in reactivity is the movement of the reaction to the outer fringe and it has the effect of decreasing the influence of Le number on the heat transfer. For decomposition of air and combustion reactions in decomposed air, the effect of Le number on the heat transfer is less than that at the frozen state.

In the study of non-equilibrium problems located between the equilibrium and frozen states, the difficulty is not in solving the boundary layer equation itself. Rather, it is difficult to provide the accurate reaction rates. When the amount of injection is not too large and near the stationary point, the difference between the equilibrium and the frozen states is not too significant. Therefore, under such condition

the non-equilibrium condition does not have to be considered.

REFERENCES

[1] Lees, L., Combustion and Propulsion, Third AGARD Colloquium, N. Y. (1958), 451—498.
[2] Emmons, H. W., Leigh, D. C., Tabulation of the Blasius function with blowing and suction, Curr. Pap. Aero. Res. Coun:, Lond. (1953).
[3] Lees, L., *Jet Propulsion*, 26(1956), 259—269.
[4] Fay, J. A., Riddell, F. R., *JAS*, 25(1958), 73—85.
[5] Vojvodich, N. S., Pope, B. B., *AIAA J.*, 2, 3(1964), 536—542.

Abstract

To simplify our problem, a stoichiometric formula is derived for boundary layers with mass injection and chemical reaction. As an example, the solution of chemical equilibrium was analized. Results of calculation were found to be in close agreement with that of experiment [5], and with that of [4] when there is no injection. Finally, it was indicated that the effect of Lewis number on heat transfer decreases as the capability of heat generating reactions increases.

THE MEASUREMENTS OF THE STATIC AND DYNAMIC STABILITY DERIVATIVES OF CONICAL MODELS IN THE SHOCK TUNNEL

Ma Jia-huan, Tang Zhong-heng, Zhang Xiao-ping and Guo Yan-ping
(Mechanics Research Institute, Academy Sinica)

Experimental research of shock tunnel for the development of hypersonic gasdynamics has been conducted widely. Due to its extremely short duration, there exist certain difficulties in the measuring technique. Hence, it is limited to the static aspect when the stability of a flying vehicle is studied. In fact, the oscillatory motion of the flying vehicle after reentry directly affects the aerodynamic load and the aerodynamic heating. Hence, the study of dynamic stability is a very essential issue. For the experimental investigation of the dynamic stability, the model free flight method which avoids completely the disturbance of the sting displays its unique superiority. Trial efforts were made in this field but have not been successful due to the short duration of the shock tunnel [1]. To extend the range of application of the shock tunnel on the one hand, and to initiate the experimental study of the hypersonic dynamic stability on the other, we spent some effort on modeling and angular measurement and obtained 1.5-2.0 cycles of pitching angle motion θ_c = 10° and 11° cones in a hypersonic flow of M_∞ = 9.0 with the model free flight method. Through data processing technique, not only their static stability derivatives are obtained, but also the preliminary result of the dynamic stability.

1. Experimental facility, measuring technique and model

The experiment is conducted in a JF-8 reflection type shock tunnel. The air flow in such a tube is motivated by the mixing and combusting of hydrogen and oxygen. The internal diameter of the shock tunnel is 150 mm and the diameter of the test section is 1.2 m. The typical operating condition for the experiment is:

Received 4 May 1979.

M_∞ = 9.0, Re_∞ = 1.6 x 10^6, and a quasi-steady operating duration of about 10 millisecond.

The first step of the free flight method for force measurement is to hang the model in the test section of the tunnel with extremely thin nylon wires at prescribed initial conditions. As soon as the initiating shock scans through the test section, the nylon wires are burnt out and the model is left exposed to the aerodynamic force and the gravity only, without any other support. The free flight motion is then satisfied. The motion of the model at this instant can be recorded by means of synchronized high speed photography. By analyzing the data and the motion of the model, the aerodynamic characteristics can be determined. The "Strobokin" high speed flasher with flashing frequency of f = 5 kc/s is used. Each single flashing pulse is about 1 sec. The motion history of the model is recorded by the revoling drum camera. The duration time of the flash is controlled by a timer and is corresponding to the quasi-steady operation time after the tunnel is started. In order to identify the flow state corresponding to each film, the measured signal of the pitot pressure in the test section of the wind tunnel and flashing signal must be recorded simultaneously on the oscilloscope (see Figure 1). The complete set up of the testing system is shown in Figure 2.

A model of very small moment of inertia of rotation is one of the basic requirements to obtain relative more periods of angular motion in the shock tunnel and hence to obtain the dynamic derivative. During the quasi-steady operating time t of the wind tunnel, the period of oscillation of the model is

$$N = \frac{t}{2\pi}\sqrt{\frac{-C_{m_\alpha} \cdot q \cdot S \cdot d}{I}} \qquad (1)$$

and within the same duration, the flight distance of the model due to drag is

$$r = \frac{C_{Deff} \cdot q \cdot S \cdot t^2}{2m} \tag{2}$$

By direct substitution, it can be observed that

$$N = \frac{1}{\pi} \sqrt{\frac{-C_{m_\alpha}}{C_{Deff}} \cdot \frac{r}{2} \cdot \frac{md}{I}} \tag{3}$$

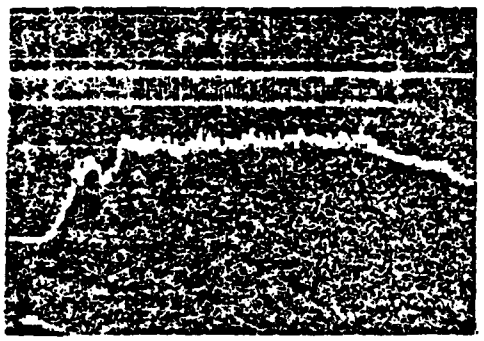

Figure 1. Pitot pressure and flashing signals
upper line: flashing impulse signal
lower line: pitot pressure signal
scanning speed: 2 ms/cm

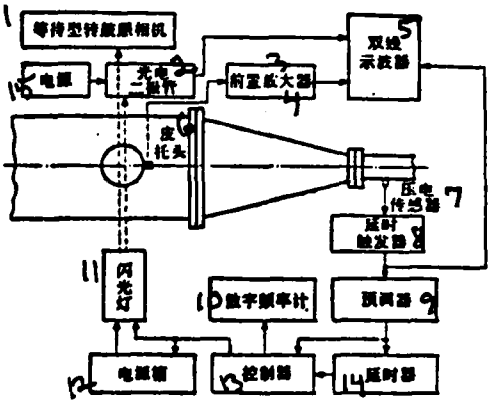

Figure 2. Schematic diagram of testing system
1-waiting-type drum camera; 2-photoelectric diode; 3- preamplifier; 4-preamplifier; 5- two-channels oscilloscope; 6- pitot head; 7- transducer; 8- trigger delayer; 9- presetting circuit; 10- digital freq. meter; 11-flash light; 12- source box; 13- controller; 14- timer; 15- electric source;

In the above equations,

t quasi-steady operation time duration

q dynamic pressure of the flow

d characteristic dimension of the model, that is, the base diameter

S the base area of the model, $S = \frac{\pi d^2}{4}$

m the mass of the model, $m = \frac{W}{g}$

I the rotational moment of inertia of the model about the lateral axis through the center of gravity

$C_{m\alpha}$ the static stability derivative of the model

C_{Deff} the effective drag coefficient of the model under the test condition

The model should be designed such that r does not overshoot the range of the camera lens while maintaining the maximum possible periods of angular motion. From Equation (3), it is observed that for a certain aerodynamic profile under a specified flow condition, the model must acquire a sufficient amount of mass with a minimal rotational moment of inertia. Hence, the structure of the model is generally composed of a heavy core with a light outer shell. The outer shell is made of very light polymer material and lead beads are used as core to regulate the position of the center of gravity of the model. The rotational moment of inertia obtained is $(1\text{-}2)\times10^{-3}$ gm-cm-sec^2. The geometrical dimension and the physical parameters of the model must be measured accurately before conducting the experiment. Typical dimensions of the conical models used in this experiment is listed in the following table (Table 1):

TABLE 1. Typical geometrical dimensions and physical parameters of the conical models

Model type	Geometrical Dimensions				Physical Parameters		
	model code	semi-vertex angle θ_c deg	length L cm	base diameter D cm	Wt. W gm	Relative ctr. of gravity x_{cg}/L	Rotational moment of inertia I gm-cm-sec
conical	10 - 7	9°57'	5.67	2.01	1.726	0.39	1.52×10^{-3}
conical	11 - 4	10°57'	5.14	1.97	1.494	0.41	1.11×10^{-3}

2. Gathering and analyzing the data

To improve the precision in the detection of the angular position of the model, the coordinated reading method is employed. 12 points are detected on the profile of the model image in the HCZ-1 three-dimensional detector and the probability error of the orientation angle is about ± 0.05°.

For the plane free flight motion of axi-symmetrical model without rotation, the law of angular motion can be written as

$$\ddot{\theta} - \left(\frac{M_q + M_{\dot{\alpha}}}{I} - \frac{q \cdot S}{m \cdot V} \cdot C_{L_\alpha}\right)\dot{\theta} - \left(\frac{M_\alpha}{I}\right)\theta = \frac{M_a}{I} \quad . \tag{4}$$

where

$M_q = M_\alpha$-- derivative of moments due to aerodynamic drag, if expressed in terms of coefficients: $(C_{mq} + C_{m_{\dot{\alpha}}}) \cdot \frac{d^2}{V} \cdot q \cdot S$

M_α -- derivative of static pitching moment $C_{m_\alpha} \cdot d \cdot q \cdot S$

M_a -- additional moment due to slight asymmetry

Reference [2] has made detailed description according to the three-cycles theory. Since under general condition,

$$\left(\frac{M_q + M_{\dot{\alpha}}}{2}\right)^2 \ll 4\left(\frac{M_\alpha}{I}\right) \tag{5}$$

Hence, after linear assumption for angular motion of single degree of freedom, Equation (4) may have solution of the following simple form:

$$\theta = K \cdot e^{\lambda t} \cdot \cos(\omega t + \delta) + K_3 \tag{6}$$

where

$$\omega^2 = \frac{-C_{m_\alpha} \cdot \pi \cdot q \cdot d^3}{4I} \tag{7}$$

$$\lambda = \frac{\left[(C_{m_q} + C_{m_{\dot{\alpha}}}) - \frac{I}{md^2} \cdot C_{L_\alpha}\right] \cdot \pi \cdot q \cdot d^4}{8I \cdot V} \tag{8}$$

As a special case of the three-cycle theory, this solution can be represented by a rotating vector with the pitching angle θ as the projection of this vector on the vertical axis. The magnitude of the vector is K. It rotates at an angular velocity of ω and δ is the initial angular position. The K_3 in Equation (6) is a small adjustment angle due to the moment M_a.

With Equation (6) and the data set of angular motion of the model $(\theta_i, t_i)_{i\ 1,2,3,\cdots,\eta}$ taken from the experiment and employing the least square method to match them, the coefficients in the equation can be determined.

The convergence criterion in the iterative matching process is

$$|SSR_2/SSR_1 - 1| < 10^{-4} \tag{9}$$

where

$$SSR = \sum_{i=1}^{\eta} \{\theta_i - [K_0 \cdot e^{\lambda_0 t_i} \cdot \cos(\omega_0 t_i + \delta_0) + K_{\dot{m}}]\}^2 \tag{10}$$

in which the subscript o indicates the first approximation value of the parameter, while 2 and 1 indicate the results obtained after two successive iteration. After the iteration is completed, the static and dynamic stability derivatives of the pitching motion of the model can be determined according to Equations (7) and (8) and the ω and λ obtained.

3. Results and discussion

Table 2 lists the experimental result of static and dynamic stability derivatives for θ_c = 10° and 11° cones at M_∞ = 9.0.

Table 2. Experimental result of static and dynamic stability derivatives for θ_c = 10° and 11° cones

test condition		$M_\infty = 9.0$, $Re_\infty = 1.6\times10^6$ 1/m		motion parameters obtained					aerodynamic derivatives		matching error	
test no.	dynamic pressure	model no.	initial angle of attack	K_1	K	λ	ω	$\frac{\omega d}{V}$	C_{m_q}	$C_{m_q} + C_{m_{\dot{\alpha}}}$	ΣR_i^2	σ
1469	0.182	10—7	6°	0.0135	0.119	−10.69	1158	0.0086	−1.76	−3.4	0.00056	0.0025
1470	0.192	10—4	10°	0.0154	0.158	−18.82	1061	0.0079	−1.62	−6.9	0.00076	0.0031
1478	0.178	10—3	12°	0.0151	0.169	−23.00	1200	0.0089	−1.75	−7.2	0.00229	0.0047
1476	0.183	10—6	16°	0.0141	0.260	−3.84	977	0.0072	−1.53	−1.2	0.00181	0.0042
1432	0.186	11—4	4°	0.0117	0.078	−9.08	1249	0.0091	−1.54	−2.2	0.00056	0.0027
1441	0.189	11—9	12°	0.0220	0.189	−15.36	1201	0.0088	−1.46	−3.9	0.00628	0.0084
1451	0.194	11—15	16°	0.0147	0.239	−12.32	1170	0.0085	−1.42	−3.2	0.00123	0.0041
1471	0.195	11—6	10°	0.0060	0.181	−12.79	1218	0.0089	−1.50	−3.2	0.00433	0.0063
1472	0.192	11—7	20°	0.0103	0.287	−10.79	1200	0.0088	−1.46	−2.7	0.00752	0.0083
1474	0.196	11—14	28°	0.0160	0.428	−12.72	1192	0.0087	−1.55	−3.5	0.00199	0.0047

The table does not only list the motion parameters and the aerodynamic stability derivative of each experiment, but also the probability error σ of matching. It reflects the deviation of mathematical model from the actual angular motion. It is given by the following expression:

$$\sigma = 0.6745 \sqrt{\frac{\sum_{i=1}^{n} (\theta_{i\text{测}} - \theta_i)^2}{n - N}} \tag{11}$$

N is the number of unknown coefficients during the matching process. Here N = 5, n is the number of data points involved in the matching.

As a typical angular motion of the model, experiment 1469 is sketched in Figure 3. The solid line in the figure shows the motion based on the substitution of the gasdynamic parameters obtained from the matching into Equation (6).

The static stability derivative $C_{m\alpha}$ indicate that within the test range, the value of $C_{m\alpha}$ is independent of the initial angle of attack. It is mainly affected by the location of the center of gravity of the model. This shows a relatively good linearity of the static stability of the conical models. The results are plotted in Figure 4 and the values are found to be consistent with Newton's theory which governs the solid line in the figure according to the following expression [3]:

$$C_{m_\alpha} = -2.083\left(\frac{\operatorname{ctg}\theta_c}{3} - \frac{x_{cg}}{2L}\operatorname{ctg}\theta_c \cdot \cos^2\theta_c\right) \tag{12}$$

The result for the dynamic stability derivative can be seen in Figure 5. It is observed that the pitching resistance moment coefficient obtained is much higher than the Newton's value and that the dispersion is relatively large for different experiments.

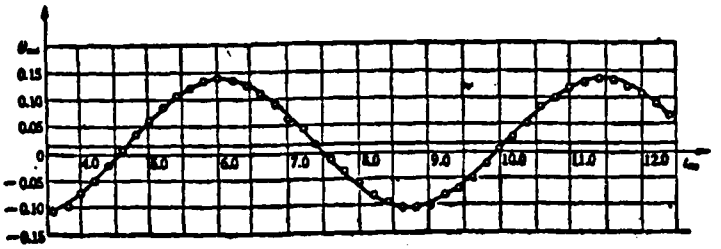

Figure 3. Typical detecting angular motion and matched angular motion
o detected motion ——— matched motion
M_∞=9.0, Re_∞=1.6x10^6/m, $\frac{\omega d}{V}$ =0.0085, test No. 1469, model no.10-7
$C_{m\alpha}$=-1.76 $C_{mq}+C_{m\dot{\alpha}}$=-3.4

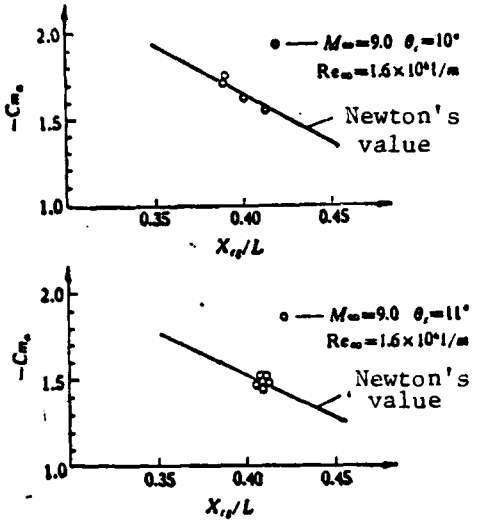

Figure 4. Experimental result of static stability for θ_c=10°, 11° cones

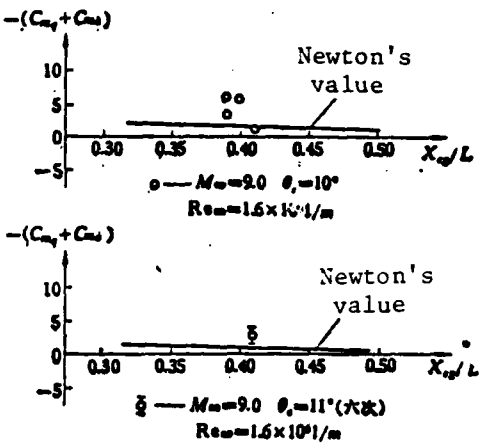

Figure 5. Experimental result of dynamic stability for θ_c=10°,11° cones

The dispersion of the experimental results is closely related to the inaccuracy in the determination of flow parameters. As indicated by Equation (8), the final value of the aerodynamic resistance coefficients, besides based on the resistance factors obtained from matching, are also determined by the dimension of model and the flow parameters. The determination of the dynamic pressure value is especially difficult due to possible error of

relative large magnitude. The general trend reflected by several sets of experimental data is much larger than the Newton's value. The causes of this phenomena requires further analysis. From the experimental result of the effect of Reynold's numbers and the decrease in frequency on the aerodynamic resistance given by [4], we observe that the dynamic stability multiplies with the increase in frequency at low Reynold's number. Hence, with $Re_D = 3x10^4$ based on the characteristic length of the model in our case and with a low frequency $f = \frac{\omega d}{V} \sim 0.01$, pitching resistance derivatives higher than the Newton's value are expected consequence. Furthermore, it should be pointed out that the models used here are not sealed at the base. Hence, there practically exists a large concave base which has a considerable effect on the aerodynamic resistance coefficient. As mentioned before, the dispersion of the resistance coefficient is quite considerable and the results are essentially preliminary. However, such dispersion does not overshoot its order of magnitude. Also, the consistency in the characteristic of the dynamic stability reflected by different experiments demonstrates the possible prospect of the measurement of dynamic derivatives with the free flight method in the shock tunnel.

REFERENCES

[1] Bixler, D. N. & Gates, D. F., Force and Moment Measurements of Models of the ARGMA Configuration in the NOL 4 in Hypersonic Shock Tunnel, No. 8, AD 270683 (1961. 11).

[2] Eikenberry, R. S., Analysis of the Angular Motion of Missles, N70-37626 (1970. 2).

[3] Scott, C. J., The Theoretical Determination of Stability Derivatives of Bodies of Revolution in Hypersonic Flows. Including Thickness Effects, A. A. S. U. Report, No. 267(1967).

[4] Urban, R. H. & Shanahan, R. J., Dynamic Stability Characteristics of a 10-Deg Cone at Mach Number 20, AEDC TR-65-80, N65-29196 (1965, 4).

LEAST SQUARES FINITE ELEMENT ANALYSIS OF STEADY HIGH SUBSONIC PLANE POTENTIAL FLOWS

Jiang Bo-nan and Chai Jia-zhen

1. Method. The fundamental dimensionless equations for steady, subsonic plane potential flow is

$$\left.\begin{aligned} &\left(1-\frac{u^2}{a^2}\right)u_x-\frac{uv}{a^2}(u_y+v_x)+\left(1-\frac{v^2}{a^2}\right)v_y=0\\ &u_y-v_x=0,\quad a^2=1+\frac{\gamma-1}{2}\left[M_\infty^2-(u^2+v^2)\right] \end{aligned}\right\} \tag{1}$$

where x and y are the orthogonal coordinates normalized by the characteristic length of the flow field, u. v and a are respectively the velocity components and the local sound speed normalized by the sound speed of the free stream, M_∞ is the free stream Mach number and γ is the specific heat ratio.

The boundary conditions depend on the particular problem. We will employ the iteration method to find the numerical solution of the quasi-linear first order partial differential equation (1). At each iteration cycle, the least square finite element method is used to solve the linearized equation set. Both the variable stiffness and the constant stiffness models are tried out. Their difference is reflected in the linearized equations, that is, the coefficients are variables with the former model but are constants with the latter.

1) Variable stiffness method. Let

$$A=\left(1-\frac{u^2}{a^2}\right),\quad B=\left(1-\frac{v^2}{a^2}\right),\quad C=\frac{-uv}{a^2} \tag{2}$$

Then Equation (1) can be rewritten as

$$Au_x+Bv_y+C(u_y+v_x)=0,\quad u_y-v_x=0 \tag{3}$$

Coefficients A, B, C are regarded as known quantities and are determined by the velocity field solved in the preceding iteration cycle. The new values of u and v are determined with the following method. Firstly, the flow field are divided into finite elements. In order to simulate boundaries of complicated profile, quadrilateral elements with eight nodal points are employed [1]. The two velocity components at each node are taken as the main unknowns. The coordinates and the unknowns of any point in the element can be expressed as

$$\begin{Bmatrix} x \\ y \end{Bmatrix} = \sum_{i=1}^{8} N_i(\xi, \eta) \begin{Bmatrix} x_i \\ y_i \end{Bmatrix}. \tag{4}$$

$$\begin{Bmatrix} u \\ v \end{Bmatrix} = \sum_{i=1}^{8} N_i(\xi, \eta) \begin{Bmatrix} u_i \\ v_i \end{Bmatrix} \tag{5}$$

where $N_i(\xi,\eta)$ is the shape function, x_i, y_i are the coordinates of the i th node of the element, u_i, v_i are the unknown velocity components of the i th node of the element.

Equation (5) is practically the expression of approximate solution of equation (1). Generally, Equation (1) are not satisfied exactly no matter how u_i and v_i are chosen. That is for any point in the element, there exist residues:

$$\left.\begin{aligned} R_1 &= \sum_{i=1}^{8} [(AN_{i,x} + CN_{i,y})u_i + (BN_{i,y} + CN_{i,x})v_i] \\ R_2 &= \sum_{i=1}^{8} (N_{i,y}u_i - N_{i,x}v_i) \end{aligned}\right\} \tag{6}$$

Employing the least square method [2], u_i and v_i are chosen such that the residues are minimized, that is to construct a second order functional (assuming that there is only one element)

$$I = \iint_{S_e} (R_1^2 + aR_2^2)\,dx\,dy \tag{7}$$

Received October 17, 1978.

In the above expression, the integration is conducted in the region S_e and α is a positive constant. Generally, $\alpha = 1$ is taken. This indicates that the continuity equation and the irrotational equation are equally important. Taking very small value of I with respect to u_i, v_i, the linear algebraic equations with respect to u_i, v_i are obtained:

$$\begin{bmatrix} [K_{11}] & & (1) \\ [K_{21}] & [K_{22}] & (对称) \\ \vdots & \vdots & \ddots \\ [K_{n1}] & [K_{n2}] \cdots & [K_{nn}] \end{bmatrix} \begin{Bmatrix} \begin{Bmatrix} u_1 \\ v_1 \end{Bmatrix} \\ \begin{Bmatrix} u_2 \\ v_2 \end{Bmatrix} \\ \vdots \\ \begin{Bmatrix} u_n \\ v_n \end{Bmatrix} \end{Bmatrix} = \begin{Bmatrix} \{F_1\} \\ \{F_2\} \\ \vdots \\ \{F_n\} \end{Bmatrix} \tag{8}$$

Key: (1) cemetery

In which the sub-matrix of the stiffness matrix of the element is

$$[K_{ij}] = \iint_{S_e} \begin{bmatrix} A^2N_{i,x}N_{j,x} + AC(N_{i,x}N_{j,y} & ABN_{i,x}N_{j,y} + ACN_{i,x}N_{j,x} \\ + N_{i,y}N_{j,x}) + (C^2 + \alpha)N_{i,y}N_{j,y} & + BCN_{i,y}N_{j,y} + (C^2 - \alpha)N_{i,y}N_{j,x} \\ \cdots\cdots\cdots\cdots\cdots\cdots & \cdots\cdots\cdots\cdots\cdots\cdots \\ ABN_{i,y}N_{j,x} + ACN_{i,x}N_{j,x} & B^2N_{i,y}N_{j,y} + BC(N_{i,y}N_{j,x} \\ + BCN_{i,y}N_{j,y} + (C^2 - \alpha)N_{i,x}N_{j,y} & + N_{i,x}N_{j,y}) + (C^2 + \alpha)N_{i,x}N_{j,x} \end{bmatrix} dxdy \tag{9}$$

The integral in the above equation is calculated numerically by 2x2 Gaussian integration formula. The sub-vector $\{F_i\}$ of the loading vector of the element is the zero vector.

For aggregates of many elements the overall rigidity matrix and the overall load vector can be obtained on the basis of normal aggregate rules. After considering boundary condition corrections, the entire set of equations can be obtained. It should be noted that the entire load vector which has undergone boundary condition correction is no longer a zero vector.

2) Constant stiffness method.

Equation (1) is rewritten as

$$u_x + v_y = f, \quad u_y - v_x = 0 \tag{10}$$

where

$$f = \left[1 + \frac{\gamma - 1}{2}(M_\infty - (u^2 + v^2)\right]^{-1}[u^2u_x + uv(u_y + v_x) + v^2v_y] \tag{11}$$

Here f is known, and is determined by the velocity field given in the preceding iteration. Taking A = B = 1, C = 0 in Equation (9), the expression for the stiffness sub-matrix of the constant stiffness method is obtained. The sub-vector of the loading vector of the element is

$$\{F_i\} = \iint_{\sigma_e} \begin{Bmatrix} fN_{i,x} \\ fN_{i,y} \end{Bmatrix} dxdy \tag{12}$$

2. Some problems in the calculation.

Since the velocity component normal to the solid boundary is zero, the inclined boundary condition is utilized, that is, at the nodal points on the solid boundary, the tangential and the normal velocity components are taken as unknowns.

The symmetry of the stiffness matrix is favorable to the calculation. The following methods are used to solve the linear algebraic equation: the triangular decomposing method of variable band width one-dimensionally stored total stiffness matrix and the elimination method.

Set f = 0 in Equations (10), and the flow field obtained by solving this incompressible problem is taken as the initial field. At all the nodal points of the field, the problem is considered convergent if the relative variation of two successive values of the dimensionless density $\rho = \left[1 + \frac{\gamma-1}{2}(M_\infty^2 - (u^2+v^2))\right]^{1/(\gamma-1)}$ is less than a given small quantity ε.

3. Numerical examples

Several typical examples are calculated with ALGOL 60 language on the TQ-16 machine.

1) Flow past a circular cylinder. The flow condition at seven times the radius of the cylinder is considered undisturbed from the free stream. One quarter of the circular cylinder is divided into 2x2 or 4x5 elements. ε is taken as 0.0001 and 0.0009 respectively. The calculated results are shown in Table 1 and Figure 1. It can be observed that even when M_∞ reaches the critical Mach number 0.42, the variable stiffness method is still converging rapidly.

Table 1. Number of iterations for flow past circular cylinder

Calculation scheme	No. of iterations \ M_∞	0.20	0.30	0.40	0.42	0.45
4 elements	constant stiffness method	2	3	8	32	no convergence
	variable stiffness method	2	3	4	4	7
20 elements	constant stiffneww method	3	6	27	no convergence	
	variable stiffness method	2	2	3	3	5

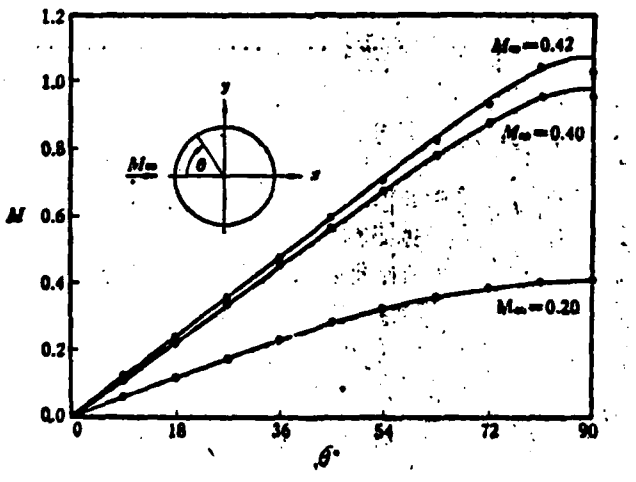

Figure 1. Mach number on the surface of the circular cylinder
o finite element (variable stiffness method)
——result from reference [3]

2) Flow past a symmetric airfoil. The symmetrical NACA 0012 airfoil with zero angle of attack is calculated. The upper half region of the airfoil is divided into 5x12 elements and $\varepsilon = 0.0001$ is taken. Convergence is achieved with the variable stiffness method after six iterations (Figure 2). There is no convergence if the constant stiffness method is used.

4. Discussion

With the above presentation, it can be concluded that the least square finite element method is feasible for steady subonic potential flows. The variable stiffness method is especially suitable for high subsonic flows.

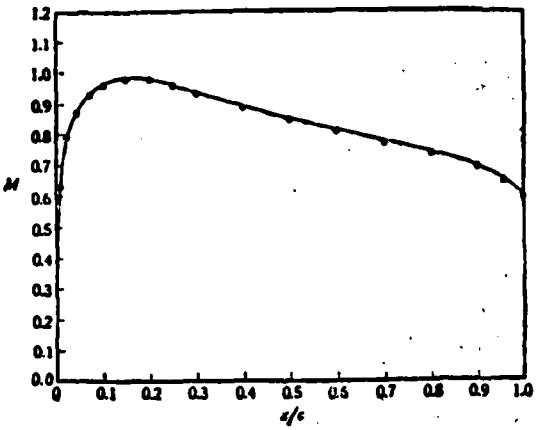

Figure 2. Mach number on the airfoil surface
o finite element (variable stiffness method)
—— result from reference [4]
NACA 0012 $M_\infty = 0.72$ 0° angle of attack

Nowadays many finite element methods [5] have been proposed for solving problems of compressible potential flows. The stream function ψ or the potential function ϕ is considered as the main unknown quantities in most methods. There are several advantages of the present method. Firstly, the velocities at the nodes are obtained directly, avoiding any numerical differentiation. Hence, relatively coarse mesh can be employed. Secondly, the difficulty

of determining the density at high subsonic Mach numbers when using ψ is also avoided. Thirdly, the boundary conditions are simpler, in contrast with the cases when ϕ is employed. Fourthly, the continuity requirement of the shape function is reduced from C' to C° as compared with the least square method for ψ or ϕ.

Finally, we thank Professor Lo Shi-jun for his valuable advice and Mr. Sun Huei-min for revising the computer program.

REFERENCES

[1] Zienkiewicz, O. C. The Finite Element Method in Engineering Science, McGraw-Hill, (1974).

[2] Edson, E. D. Int. J. Num. Meth. Engng., 10(1976), 1021.

[3] Imai, I. Proc. Phys. Math. Soc. Japan, 23(1941), 180.

[4] Lock, R. C. Test cases for numerical methods in two-dimensional transonic flows, AGARD-R-575 (1970).

[5] Shen Shen-pu. Ann. Rev. Fluid Mech., 9(1977), 421.

THE AERODYNAMICAL ANALYSIS OF BODY IN HYPERSONIC SOURCE FLOW FIELD

Ling Guo-can
(Institute of Mechanics, Academia Sinica)

The hypersonic source flow field is a typical non-uniform free stream flow field. Many high speed, high enthalpy experimental systems, such as shock tunnels equipped with conical nozzles, the gun wind tunnels, the electric arc wind tunnels, etc., are characterized by hypersonic spherical expansion. Certain external flows around bodies also display the same characteristics. Simple but accurate analytical methods are required to determine the aerodynamic force on the body and the effects on the pressure distribution and various aerodynamic characteristics for such non-uniform free stream condition. Some efforts have been made [1-7] but no satisfactory analytical results have been presented so far. Based on the characteristics of the hypersonic source flow field and the simple form of the potential function, the present study obtained various aerodynamic coefficients by means of Newton's theory. Under the condition of small angle of attack, the analytical results are satisfactory. Due to practical requirements, analysis on the effects of the non-uniformity of the free stream is emphasized. Agreement between the calculated results and the experimental data is satisfactory.

1. Hypersonic source flow field

At hypersonic conditons, $M>>1$, and when $M^2(\gamma-1)/2>>1$, the following relations among physical properties in steady, ideal point source flow are obtained by integrating the basic equations:

$$V = \text{constant}, \quad p = p_0(r/r_0)^{-2r}, \quad \rho = \rho_0(r/r_0)^{-2}, \quad M = M_0(r/r_0)^{r-1} \tag{1}$$

when r is the distance of any point in space from the point source.

The subscript denotes certain reference values in the flow field. Note that the velocity of the above flow field is almost constant. Hence, the corresponding potential function varies with r only, that is $\Phi = rV + C$. This potential function provides some convenience for the analysis following. If the point source is located at the coordinates $(\xi, 0, \zeta)$, on the symmetric surface xoz of the Cartesian coordinates Oxyz, then the velocity potential and the velocity distribution should be:

$$\left.\begin{aligned} &\Phi = V\sqrt{(x+\xi)^2 + y^2 + (z+\zeta)^2} + C \\ &V_x = (x + L_0\cos\alpha)VL^{-1}, \quad V_y = yVL^{-1}, \quad V_z = (z + L_0\sin\alpha)VL^{-1} \\ &L = \sqrt{(x + L_0\cos\alpha)^2 + y^2 + (z + L_0\sin\alpha)^2} \end{aligned}\right\} \quad (2)$$

in which L_o is the distance from the point source to the origin, and α is the angle between L_o and the x-axis.

2. Pressure distribution

Let the geometry of the body of revolution in the flow field described above be $r_b = f(x)$, and the unit vector normal to the body surface be $\mathbf{n}_b = \sin\delta\mathbf{i} - \cos\delta\cos\beta\mathbf{j} - \cos\delta\sin\beta\mathbf{k}$, $\delta = \mathrm{tg}^{-1}(dr_b/dx)$. The elevation angle of the line joining the point source and the vortex of the body from the Ox-axis is defined as the angle of attack α of the non-uniform free-stream. The Newton's hypersonic impulse theory gives the pressure coefficient, $C_{p_b} = \rho_b(\mathbf{V}_b \cdot \mathbf{n}_b)^2/q_b$, of any point on the upwind surface of the body. The subscript b denotes the local freestream parameters at any point on the body surface given by Equations (1) and (2), and x,y,z satisfy the equation of the body profile. $q_o = \rho_o V^2/2$ is the local free stream dynamic pressure at the vertex of the body. If the distance L_o from the point source to the body vertex is taken as the characteristic length of the flow and the reference value for normalization, then the pressure coefficient at any point on the upwind surface of the body is

$$C_{p_1} = \frac{2[(\bar{x} + \cos\alpha)\bar{f}' - \bar{f} - \sin\alpha\sin\beta]^2}{(1 + \bar{f}'^2)[1 + \bar{x}^2 + 2\bar{x}\cos\alpha + \bar{f}^2 + 2\bar{f}\sin\alpha\sin\beta]^2} \qquad (3)$$

Apparently, when the point source is infinitely far away from the body, the above expression reduces down to the well-known Newton's formula of the uniform flow.

For conical bodies $\bar{f} = \bar{x}\,\mathrm{tg}\,\theta$, and the pressure distribution on the conical surface is

$$\left.\begin{aligned} C_{p_1} &= C_{p_U}\bar{L}^{-4}, \quad C_{p_U} = 2[\cos\alpha\sin\theta - \sin\alpha\cos\theta\sin\beta]^2 \\ \bar{L} &= [1 + \bar{x}^2 + 2\bar{x}\cos\alpha + \bar{x}^2\mathrm{tg}^2\theta + 2\bar{x}\,\mathrm{tg}\,\theta\sin\alpha\sin\beta]^{\frac{1}{2}} \end{aligned}\right\} \qquad (4)$$

The subscript U denotes the uniform free stream values. Hence, there exists a simple transformation relation between the pressure coefficient on the conical surface in source flow field and the pressure coefficient in the corresponding uniform flow field. The former can be expressed as a function of the uniform flow values and $\bar{L}$, the dimensionless distance from the point source to the conical surface. The pressure coefficient decreases along the conical surface, hence losing the characteristics of conical flows. This effect is greater when the point source is closer to the body.

For a spherical surface of radius $\bar{f}^2 = \bar{R}^2 - (\bar{R} - \bar{x})^2$, . At zero angle of attack, the pressure coefficient on the upwind surface is

$$C_{p_1} = \frac{2[\bar{R}(\sin\theta - 1) + \sin\theta]^2}{[1 + 2\bar{R}(1 - \sin\theta) + 2\bar{R}^2(1 - \sin\theta)]^2} \qquad (5)$$

where θ is the circumferential angle as shown in Figure 2. At the stagnation point, $\theta = \pi/2$. The region of action is $\sin^{-1}[\bar{R}/(1 + \bar{R})] \leq \theta \leq \pi/2$.

Figures 1 and 2 present the calculated relative values $(C_{p_U} - C_{p_1})/C_{p_U}$ and $C_{p_1}/C_{p_{\theta=\frac{\pi}{2}}}$ of the pressure distribution on the conical surface and the spherical surface respectively.

This paper was received on December 18, 1978.

1) This paper was presented at the Chinese Institute of Mechanics' First Convention of Shock Tunnel, November 4-12, 1978.

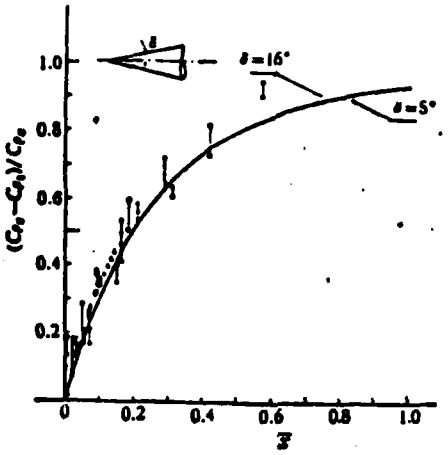

Figure 1. Pressure distribution on the conical surface (α=0°)
——calculated values according to Equation (4)

▲ $M=10.31$	$\delta=16°$	gun wind tunnel experiment [9]
○ $M=9.5$	$\delta=15°$	shock tunnel experiment (large cone) [3]
● $M=9.5$	$\delta=15°$	shock tunnel experiment (small cone) [3]
◆ $M=8.7$	$\delta=10°$	shock tunnel experiment
■ $M=7.5$	$\delta=15°$	shock tunnel experiment (large cone) [3]
□ $M=7.5$	$\delta=15°$	shock tunnel experiment (small cone) [3]

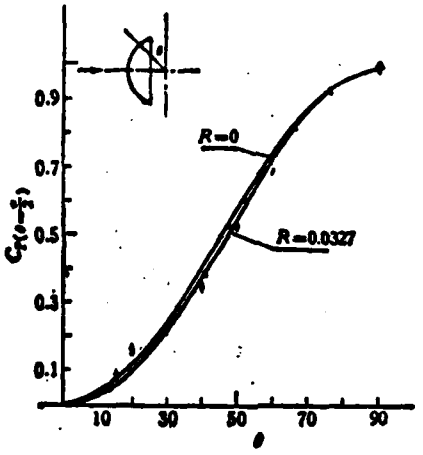

Figure 2. Pressure distribution on the spherical surface (α=0°)
——calculated values according to Equation (5)

● $R=0.009$	$M=15.9$	sphere-cylinder experiment [5]
◆ $R=0.0327$	$M=8.6$	sphere-cone experiment
▲ $R=0.0302$	$M=10.31$	sphere-cone experiment [9]

3. Aerodynamic coefficients of typical bodies

By applying the coefficient formula (3) obtained, the normal force coefficient, axial force coefficient, pitching moment coefficient and the pressure center coefficient of the body of revolution at any angle of attack can be calculated directly:

$$\left.\begin{aligned} C_{N_i} &= -\frac{2}{\pi \bar{r}_B^2}\int_0^{\bar{x}_p}\int_0^{\beta_p} C_{p,\bar{l}} \sin\beta d\beta d\bar{x}, \quad C_{T_i} = \frac{2}{\pi \bar{r}_B^2}\int_0^{\bar{x}_p}\int_0^{\beta_p} C_{p,\bar{l}}\bar{r}\bar{r}' d\beta d\bar{x} \\ C_{m_i} &= -\frac{2}{\pi \bar{r}_B^2 l}\int_0^{\bar{x}_p}\int_0^{\beta_p} C_{p,\bar{l}}(\bar{x}+\bar{r}\bar{r}')\sin\beta d\beta d\bar{x}, \quad \bar{x}_{c_{p_i}} = C_{M_i}/C_{N_i} \end{aligned}\right\} \tag{6}$$

where $\bar{x}_{c_p} = x_{c_p}/l$, l and r_B are the body length and the base radius respectively. The upper limits of the integrations $\bar{x}_p, \beta_p$ are the dividing line of the upwind and downwind surfaces and are determined by the zero pressure condition on the body surface. For conical bodies, $\alpha \leqslant \delta$, $\beta_p = \pi/2$, $\bar{x}_p = l$; $\alpha > \delta$, $\beta_p = \sin^{-1}(\mathrm{tg}\,\delta/\mathrm{tg}\,\alpha)$, $\bar{x}_p = l$. For spherical bodies, $\beta_p = \sin^{-1}\{[\bar{R}\cos\alpha - (\bar{R}+\cos\alpha)\bar{x}][\bar{R}^2 - (\bar{R}-\bar{x})^2]^{-\frac{1}{2}}(\sin\alpha)^{-1}\}$, For small angle of attack when $\bar{x}/\bar{R} \leqslant (1+\bar{R})^{-1}$ 时 $\beta_p = \pi/2$.

For small angle of attack, the higher order terms of α can be neglected. Also when the point source is considerably far from the body, the distance of any point on the body from the point source is almost equal to its projection on the x-axis. Simple analytical expressions for aerodynamic coefficients are obtained through integration. The position of the point source still has a sufficiently large range in these expressions. For cones at $\alpha \leqslant \delta$, there are certain correlations between the aerodynamic coefficients in the point source flow field and the corresponding coefficients in the uniform flow. The normal force coefficients, axial force coefficients, static derivative $C_{N\alpha}$, pressure center coefficient, pitching moment coefficient in the point source flow field can all be expressed by the product of the corresponding value in the uniform flow field and the correlation function $\varphi_i(l)$

$$C_{N_l} = C_{NU}\varphi_1(l), \quad C_{T_l} = C_{TU}\varphi_1(l), \quad C_{N\omega_l} = C_{N\omega U}\varphi_1(l)$$
$$\bar{x}_{C_{pl}} = \bar{x}_{C_{pU}}\varphi_2(l), \quad C_{m_l} = C_{mU}\varphi_1(l)\varphi_2(l) \qquad (7)$$

$$C_{NU} = 2\alpha\cos^2\delta, \quad C_{TU} = (\alpha^2 + 2\mathrm{tg}^2\delta)\cos^2\delta, \quad C_{N\omega U} = 2\cos^2\delta$$
$$\bar{x}_{C_{pU}} = 2/3\ \sec^2\delta, \quad C_{mU} = 4/3\ \alpha \qquad (8)$$

$$\varphi_1(l) = (3 + l)/3(1 + l)^3, \quad \varphi_2(l) = (1 + 1/3\,l)^{-1} \qquad (9)$$

The correlation functions $\varphi_1(l), \varphi_2(l)$ depends on the dimensionless characteristic quantity l, only, which denotes the relative position of the body in the point source flow field. Figure 3 shows the variation curve of $1 - \varphi_1(l)$ versus l. The relative variation of the aerodynamic coefficients due to the non-uniformity of the free stream under the condition of different point source positions can be determined according to this curve.

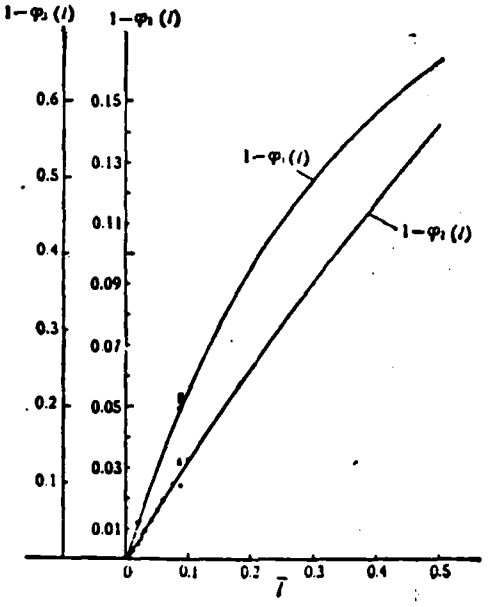

Figure 3. $1 - \varphi_1(l)$ curve

SYMBOL	CONTENT	$\bar{\eta}$	$\bar{\delta}^\circ$	$\bar{\alpha}^\circ$	M	Ref
●	pressure center experiment	0	7	small	16	5
♦	pressure center experiment	0	6	small	20	5
■	pressure center experiment	0	10	7,5,10	8.2	
○	pressure center modification calculation	0	small	small		5
▲	pressure center modification calculation		16	2-15		7
▼	normal force coefficient experiment	0	7	5	16	5
□	axial force coefficient modification calculation	0.006	16	2-15		7
▽	normal force coefficient modification calculation	0.006	16	2-15		7

For the spherical section and for $l_* \leqslant (1+\bar{R})^{-1}$, the following expressions can be obtained after some complicated integrations:

$$\left.\begin{aligned} C_{N_1} &= \frac{a}{4\bar{R}^4(1+\bar{R})^3(2-l_*)l_*}\left\{R_1 + R_2 l_* + R_3 \ln[1+2\bar{R}(1+\bar{R})l_*] + \frac{R_4}{1+2\bar{R}(1+\bar{R})l_*} + \frac{R_5}{[1+2\bar{R}(1+\bar{R})l_*]^2}\right\} \\ C_{T_1} &= \frac{1}{4\bar{R}^4(1+\bar{R})^3(2-l_*)l_*}\left\{S_1 + S_2 l_* + S_3 l_*^2 + S_4 \ln[1+2\bar{R}(1+\bar{R})l_*] + \frac{S_5}{1+2\bar{R}(1+\bar{R})l_*}\right\} \\ C_{m_1} &= C_{N_1} l_* \end{aligned}\right\} \quad (10)$$

where

$$\left.\begin{aligned} &R_1 = 2.5 + 14\bar{R} + 28\bar{R}^2 + 24\bar{R}^3 + 8\bar{R}^4, \quad R_2 = 2\bar{R}(1 + 3\bar{R} + 2\bar{R}^2) \\ &R_3 = -(3 + 12\bar{R} + 16\bar{R}^2 + 8\bar{R}^3), \quad R_4 = -(3 + 18\bar{R} + 40\bar{R}^2 + 40\bar{R}^3 + 16\bar{R}^4) \\ &R_5 = 0.5 + 4\bar{R} + 12\bar{R}^2 + 16\bar{R}^3 + 8\bar{R}^4 \\ &S_1 = 1 + 7\bar{R} + 20\bar{R}^2 + 30\bar{R}^3 + 24\bar{R}^4 + 8\bar{R}^5, \quad S_2 = 4\bar{R} + 20\bar{R}^2 + 32\bar{R}^3 + 20\bar{R}^4 + 4\bar{R}^5 \\ &S_3 = -(2\bar{R}^2 + 6\bar{R}^3 + 6\bar{R}^4 + 2\bar{R}^5), \quad S_4 = -(3 + 15\bar{R} + 28\bar{R}^2 + 24\bar{R}^3 + 8\bar{R}^4) \\ &S_5 = -(1 + 7\bar{R} + 20\bar{R}^2 + 30\bar{R}^3 + 24\bar{R}^4 + 8\bar{R}^5) \\ &\bar{R} = R/L_0, \quad l_* = l_*/R \end{aligned}\right\} \quad (11)$$

l_n is the thickness of the spherical body in the x-direction. When $\bar{R} \to 0$, the above limits become the Newton's formulae in the uniform flow. Figure 4 shows the variation curve of the derivatives of normal force coefficient and axial force coefficients of the spherical section vs. the point source position.

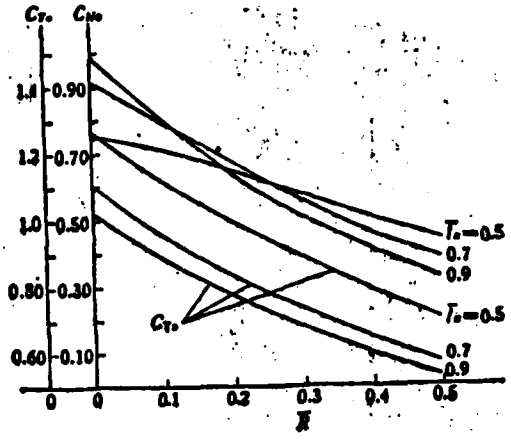

Figure 4. $C_{N\alpha}$ and C_{Ts} of the spherical section

For a slender cone-sphere combination of bluntness η at $\alpha \leq \delta$, and for $\sin\delta \sim \delta$, $\cos\delta \sim 1$, the following can be obtained:

$$\left.\begin{aligned} &C_{N\text{con}_s} = C_{N\alpha_s}\eta^2 + C_{NB_s},\quad C_{T\text{con}_s} = C_{T\alpha_s}\eta^2 + C_{TB_s},\quad C_{N\text{con}_s} = C_{N\alpha_s}\eta^2 + C_{NB_s} \\ &\bar{x}_{C_p\text{con}_s} = \left[C_{m\alpha_s}\frac{\eta^3\delta(1-\delta)}{1-\eta(1-\delta)} + C_{mB_s}\right] \Big/ C_{N\text{con}_s} \end{aligned}\right\} \quad (12)$$

and

$$
\left.
\begin{aligned}
C_{NB_1} &= \frac{2}{3}\alpha K_1(\eta, \bar{R}_B/\delta)Q^2(\eta, \bar{R}_B, \delta) \\
C_{TB_1} &= \frac{1}{3}(\alpha^2 + 2\delta^2)K_1(\eta, \bar{R}_B/\delta)Q^2(\eta, \bar{R}_B, \delta) \\
C_{mB_1} &= C_{NB_1}\bar{x}_{C_pB_1} \\
\bar{x}_{C_pB_1} &= \frac{2}{3}\frac{K_2(\eta, \bar{R}_B/\delta)}{K_1(\eta, \bar{R}_B/\delta)}\frac{1}{1-\eta(1-\delta)} - \frac{\eta(1-\delta)}{1-\eta(1-\delta)} \\
K_1(\eta, \bar{R}_B/\delta) &= \frac{(3+\bar{R}_B/\delta)}{(1+\bar{R}_B/\delta)^3}\left[1 - \frac{\eta^2(3+\eta\bar{R}_B/\delta)(1+\bar{R}_B/\delta)^2}{(3+\bar{R}_B/\delta)(1+\eta\bar{R}_B/\delta)^3}\right] \\
K_2(\eta, \bar{R}_B/\delta) &= 3\left[\frac{1}{(1+\bar{R}_B/\delta)^3} - \left(\frac{\eta}{1+\eta\bar{R}_B/\delta}\right)^3\right] \\
Q(\eta, \bar{R}_B, \delta) &= \left[1 - \eta\bar{R}_B\left(\frac{1-\delta+\delta^2}{\delta}\right)\right]^{-1}, \quad \bar{R}_B = \bar{R}_n/\eta
\end{aligned}
\right\} \qquad (13)
$$

The above results indicate that the aerodynamic coefficiencies of a slender cone sphere of definite profile in the point source flow field at small angle of attack depend only on the dimensionless parameter $\bar{R}_n$ (or $\bar{R}_B$), which characterizes the relative position of the body in the point source flow field.

4. Comparison of the results

Figures 1-3 and Figures 5 and 6 show the comparison between calculation results and the experimental data. The force measurement accuracy of current impulsive wind tunnel (about 5-10%) is one order of magnitude lower than that of the ordinary wind tunnel. Some of them reach around 17%. Since there is a lack of experimental data for single spherical section, Figure 2 adopts the results from the sphere-cone and the sphere-cylinder. Hence, the data close to the stagnation point at the head should be taken. The accurate solution of the pressure distribution on the cone of the uniform flow is taken from [10]. The pressure distribution and the relative variation of aerodynamic coefficients due to hypersonic point source free stream calculated here are found to match with the experimental results. The calculated aerodynamic coefficients of the sphere-cone combination also agree quite well with the experimental results. They are also consistent with the modified values given by [5,7]. Compared with the uniform free stream condition, the source flow causes the pressure center of the sphere-cone to move forward and the normal and axial force coefficients to decrease. For slender

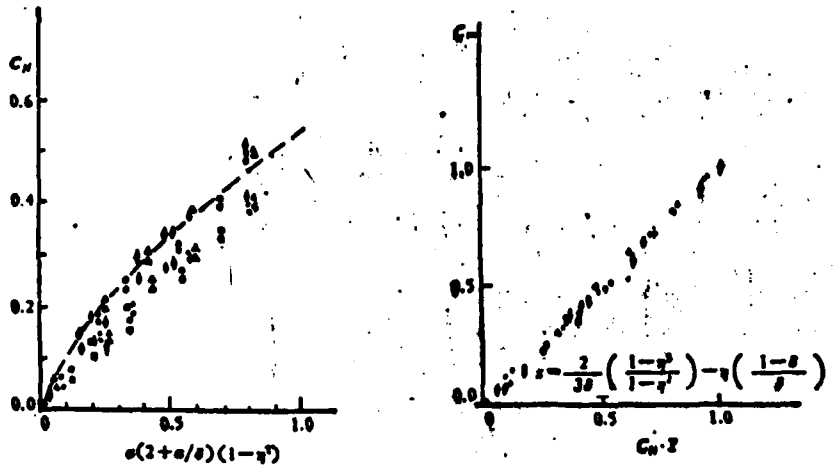

Figure 5. Normal force coefficient and pitching moment coefficient of sphere-cone

♦ calculation by Equations (12), (13)
● gun-wind tunnel experiment [7] δ =12.5° η =0-0.5 α=2-15°
▲ gun wind tunnel experiment [7] δ =16° η =0-0.5 α=0-16°
■ gun wind tunnel experiment [7] δ =20° η =0-0.5 α=0-17°
◇ uniform flow values modified by the present method
o uniform flow values modified by [7]
▲ uniform flow values modified by [7]
□ uniform flow values modified by [7]
——experimental values of uniform flow [12]

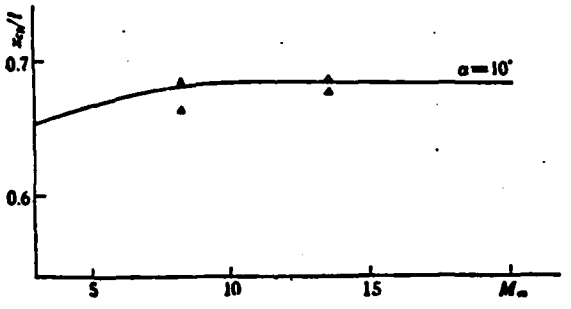

Figure 6. Pressure center of sphere-cone

▲ shock tunnel experimental values
Δ pressure center of the uniform flow modified by the present method
η=0.15 α=10° M=8.2, 13.5 η=0.15 α=10° M=8.2, 13.5
——calculated value according to the uniform flow theory
η=0.15 α=10°

cones at small angle of attack, the pressure center moves forward by $1-\varphi_2(l)$. When $l>0.03$, that variation is more than 1%. The relative variation of both the normal and axial force coefficients is $1-\varphi_1(l)$. When $l>0.04$, the variation is more than 10%. For the hypersonic uniform free stream problem, the Newton's theory is effective in determining the pressure distribution and aerodynamic coefficients, provided that the shock stays close to the body surface [11,12]. For hypersonic source flow field, it also displays a satisfactory accuracy in analyzing the aerodynamic effects due to the non-uniformity of free stream.

REFERENCES

[1] Yasuhara, M., et al. AIAA J., 15 12(1977), 1667-1668.

[2] Lin, T. C., et al. AIAA J., 15 8(1977), 1130-1137.

[3] Inouye, M., NASA TN-D 3382(1966).

[4] Crowell, P. G. SAMSO-TR-70-302 (1970).

[5] Pate, S. R., et al. AIAA paper 74-84.

[6] Soga, Kunio et al. N73-14978 (NAL TR-280).

[7] Wada, Isamu et al, Journal of Japanese Institute of Aeronautics and Astronautics, 23, 262(1975), 35-41.

[8] Yasuhara, M., et al. Modern Development in Shock Tube Research, Proceedings of the 10th International Shock Tube Symposium (1975), 446-451.

[9] Soga, Kunio et al, Journal of Japanese Institute of Aeronautics and Astronautics, 25, 283(1977), 14-22

[10] Ames REs. Staff, NACA Rept. 1135 (1953).

[11] Ladson, L., et al. NASA TN-D-1473 (1962).

[12] Whitfield, J. D., et al. AEDC-TDR-62-166 (1962).